Republic of Iraq
Ministry of Higher Education & Scientific Research
University of Babylon
College of Education for Pure Sciences
Department of Physics

Effect of Coupled Channels in Elastic and Inelastic Scattering of Weakly Bound Nuclei for some Selected Systems

A Thesis

Submitted to the Council of the College of Education for Pure Sciences University of Babylon in Partial Fulfillment of the Requirement for the Degree of Master in Education / Physics

By

Eman Dabul Abdul-Hamza Kazim

B.Sc. in physics

University of Babylon, 2014

Supervised by

Professor
Dr. Fouad A. Majeed
College of education for pure sciences
Department of physics

Assistant Professor
Dr. Fatima M. Hussain
College of education for pure sciences
Department of physics

2021 A.D 1443A.H

بِسْمِ اللهِ الرَّحمٰنِ الرَّحِيمِ

﴿ يَرْفَعِ اللَّهُ الَّذِينَ آمَنُوا مِنْكُمْ
وَالَّذِينَ أُوتُوا الْعِلْمَ دَرَجَاتٍ وَاللَّهُ
بِمَا تَعْمَلُونَ خَبِير ﴾

صَدَقَ اللهُ العَلِيُّ العَظِيمُ
سورة المجادلة/ آية 11

Datication

To my first teacher... to my father's spirit

To

my mother

To

my brothers and sisters…

To

my friends..

For their kindness attention

and encouragement…

Acknowledgements

Praise is to *Allah*, Mercy and peace are to the Prophet Mohammed and his relatives and companions.

First, I would like to express my deep gratitude and appreciation to my supervisor, **Prof. Dr. Fouad A. Majeed** for suggesting this project, guidance, support, and encouragement through the research work.
Second, I am deeply indebted to my supervisor **Asst. Prof. Dr. Fatima M. Hussain**, for her endless trust and support. Her continuous guidance, meticulous scientific suggestions, and for her inexhaustible patience during the practical phase helped me in all the time of research and writing of this thesis.

Thanks to the deanery of the college of education for pure sciences-Babylon university and the department of physics for offering me the opportunity to complete my research. I also would like to express grateful to all teachers, instructors and students of department of physics for their assistance and supports specially.
It gives me immense pleasure to thank **Mr. Yousif Abdul-Hakeem Abdul-Hussein** from the Department of Physics of the College of Education for Pure Sciences, for his assistance, which has always played a key role in the scientific developments of the present thesis, and his support during the development of all the programming codes of this thesis, wishing him endless success in his life.

Finally, I am truly thankful for the tremendous support from my family.

Abstract

In this thesis, the calculations of the total nuclear scattering cross-section (elastic and inelastic) and the distribution of the Coulomb barrier are taken of Weakly Bound nuclei for some selected systems, ^{6}He + ^{120}Sn, ^{6}Li + ^{64}Zn, ^{7}Li + ^{64}Zn, ^{8}B + ^{58}Ni, ^{9}Be + ^{64}Zn, ^{12}C + ^{208}Pb, ^{6}He+^{58}Ni and ^{11}Be+^{197}Au . The effect of channels coupling with breakup channel on the calculations of the ratio of total scattering cross section to Rutherford cross section σ_T/σ_R and the distribution of the Coulomb barrier D_{el} (MeV^{-1}) have been achievement. The optical nuclear potential has been described by using Wood-Saxon (WS) potential. Which has (real and Imaginary) parts, the parameters of this potential are depth, radius and surface nuclear diffuseness parameter. The Wood-Saxon parameters for Akyüz-Winter potential were taken by least-squares method to experimental data of scattering cross sections by sub-Code program written in Fortran 90 language.The program Code (CC-SCT) coupled channel scattering for windows which is considered the latest version of computer Code CC has been coded by Fortran 90 language. This program Code (CC) coupled channel is studied the Coulomb excitations of scattering reactions of nuclei in full quantum mechanics by using Continuum-Discretized Coupled Channels (CDCC) method of Alder and Winther theory(AW). The calculations of the ratio between the cross section of nuclear scattering to Rutherford scattering as a function of the center of mass angle θ_{cm} and the center of mass energy E_{cm} as well as calculating the elastic scattering barrier distribution D_{el} as a function of energy in no-coupled and coupled channel states, where thise calculations were found in good agreement with available experimental data of the role coupling with breakup channel. The best fitted values of

the parameters have been implemented for the calculations through a good agreement between these calculations with the experimental data.

Contents

List of Figures

List of Tables

List of Symbols

Symbol	*Physical Meanings*
v	The asymptotic relative velocity.
A_P,A_T	The mass number for projectile and target.
$\upsilon_{n0,cm}$	The initial velocity of a neutron in a center-of-mass system.
υ_{n0}	Initial neutron velocity in a laboratory system.
ψ	The scattered wave function.
$E_{c.m}$	Energy for the system center-of-mass.
E_{lab}	The kinetic energy in the laboratory system.
E_{exc}	the excitation energy.
b	Impact parameter.
d	distance of closest approach.
d_0	minimum for a central collision
F_C	The Coulomb force.
C	Constant.
r	System relative distance.
l	The orbital angular momentum.
m_P, m_T	The mass of the projectile nuclei and The mass of the target nuclei.
ε_0	vacuum permittivity
Z_P, Z_T	The atomic number for the projectile nuclei and The atomic number for the target nuclei.
$\frac{d\sigma}{d\Omega}$	The differential scattering cross section.
$d\Omega$	The solid-angle element.
h	Planck constant.
r_o	The radius parameter.
$\hbar$	reduced Planck constant.
μ	The reduced mass.
$f(\theta,\emptyset)$	The scattering amplitude.
R_e	stands for the real part.
j_i	The probability current density
da	The effective area.
J_{sc}	The probability current density for the scattered spherical wave.

σ_{sc}	Cross section of elastic scattering.
a_l	the expansion coefficients
a_0	The diffuseness parameter.
δ_l	The phase shift.
$p(x)$	The linear momentum.
θ	Polar angle.
$\emptyset$	Azimuthal angle.
u_l	the modified radial wave function
k	The incident wave vector.
$\acute{K}$	The scattered wave vector.
P_l	The Legendre polynomial.
$V(R)$	The interaction Potential.
$\frac{e^{ikr}}{r}$	The spherical wave.
$f(\theta, \emptyset)$	The scattering amplitude.
A_l , B_l, C_l	Constants.
$\hat{r}$	The radial unit vector.
$j_l(kr)$	The spherical Bessel function
Y_{l0}	spherical harmonic function
η_l	reflection coefficient
σ_{sc}	The scattering cross section
V_N	The nuclear potential.
R_0	radius of the system.
V_0	The depth of the potential.
V_C	The Coulomb potential.
V_B	The height of the Coulomb barrier.
R_C	The radius of system charge sphere.
r_c	Coulomb radius parameter.
V_{eff}	effective potential.
τ	for the set of intrinsic coordinates of the projectile and target nuclei.
H	Hamiltonian.
H_0	intrinsic Hamiltonian.
T	kinetic energy operator of the relative motion between the projectile and target nuclei.
U	the interaction potential.
η	The eigenstates of the intrinsic Hamiltonian.
U'	Represents the diagonal elements.
U''	Represents the non-diagonal elements.

e_η	The total internal kinetic energy.
$\Re_{tot}(\theta, E)$	The amplitude of scattering.
$\Re_N^{(\eta)}(\theta, E)$	nuclear amplitude of scattering.
$\Re_C(\theta, E)$	Coulomb amplitude of scattering.
R_b	The position of the Coulomb barrier.
R_N	The radius of the nuclear potential.
σ_R	the Rutherford cross section.
$D_{tot}(E)$	The scattering barrier distribution
S_l	The nuclear *S*-matrix.
$D_{fus}(E)$	the barrier of fusion.
S.C	Single Channel.
CC	Coupled Channel.
WS	Wood-Saxon.
AW	Winther theory.
CC-SCT	coupled channel scattering.
CDCC	Continuum Discretized Coupled Channel formalism.
HI	heavy ion.
BTA	Breakup Threshold Anomaly.
TA	Threshold Anomaly.

Chapter One

Introduction and Literature Survey

1.1 Introduction

The study of the collisions of weakly bound nuclei for both stable and radioactive ones, at near barrier energies became one of the most important fields in the modern nuclear researches nowadays. The nuclear reaction takes place by the collision of two nuclei to produce products different from the initial ones [1].The processes associated with this reaction can be understood by the devoting of the theoretical and experimental efforts, by taking into account the couplings between them [2]. And that will help to understand the nuclear properties of the ingredients of our universe by collecting a wide spectrum of different reaction modes lies between the elastic scattering and the fusion reaction, and these reactions are strongly relevant to each other as proved during the past few years [3, 4]. In addition to the transfer channels for the halo nuclei, breakup channel plays an important role in the collisions of a weakly bound systems. The breakup cross-section of the weakly bound nuclei is large because of their low breakup threshold, and that will have influence on other reaction channels [5].

In collision between two ions, the process that brings them to form a single composite system is called fusion. The simplest description of this process considers the two ions as rigid spherical objects that interact via a repulsive, Coulomb, plus an attractive, nuclear, potentials depending only on the relative center-of-mass (c.m.) distance. Fusion is described as the ability of the system to penetrate the potential energy barrier [6, 7]. However, many experiments have shown that the barrier penetration model is inadequate for the description of the observed cross sections, at energies below the Coulomb barrier the model under predicts, of several orders of magnitude, the observed values [8]. These discrepancies have been readily attributed to the effect of coupling of the relative motion to

the internal degrees of freedom of the two colliding ions. The factors that have been identified as playing a major role in the enhancement of the sub-barrier fusion are permanent nuclear deformation, coupling to the low-lying nuclear excited states, and possibly, particle transfer (in particular neutrons) [9].

1.2 Types of nuclear reactions

1.2.1 Elastic scattering

In this type of reaction, the target nucleus (X) is left in its ground state, there is no change in the potential energy, and of course the projectile and ejectile are the same. The only difference is that the kinetic energy of the ejectile will be less than that of the projectile [10,11,12], the general representation of this type of reaction is:

$$^{A}X\ (a,a)\ ^{A}X$$

1.2.2 Inelastic scattering

Inelastic scattering is the process by which, the target nucleus is left in an excited state, i.e. both projectile and target are kept their identity, except that the product nucleus is in an excited state with respect to the target which be in the ground state [10,11,12], the general representation of this type of reaction is:

$$^{A}X\ (a,a)^{A}X^{*}$$

1.2.3 Evaporation reaction

In this type of reactions, there is more several ejectile particle, and these may be protons, neutrons or their combinations as alpha particles [10].

1.2.4 Transfer reaction

When the projectile takes nucleons from the target, the transfer reaction is called pickup reaction, while when the projectile loses

nucleons to the target, the transfer reaction called stripping reaction [10,11].

1.2.5 Fission reaction

When the target nucleus excited by the projectile, it may be breakup into two nuclei with comparable mass.

1.2.6 Fusion reaction

In nuclear physics, fusion process is a reaction in which two or more atomic nuclei are fused to form a new heavier nucleus. An example is the fusion of hydrogen nuclei to form helium nucleus, which is a familiar type of fusion reactions happen in stars, thus it has a special importance in evolution of the universe [10,13,14]. In the field of reaction theory, the fusion process is defined as the reaction of two separated nuclei to form a compound nucleus (C) as a result of overcoming on the Coulomb barrier by accelerate one nucleus called projectile (x) into another nucleus in principle at rest called the target (A).

$$x+A\rightarrow C \qquad (1.1)$$

Thus the fusion reaction in interest is not a chain reaction like that happened in stars [14]. The compound nucleus itself is not a stationary state on the macroscopic time scale, but it stills a long time in nuclear time scale [14,15].

1.2.7 Compound nuclear reaction

Here the compound nucleus occurs as intermediate stage, before either evaporation or fission, the compound nucleus has a lifetime about $\sim 10^{-16}$ sec, and when this time was compared with the time that taken by the projectile to cross the target nucleus, it can be say that the compound nucleus does not depend on the way it was formed [11,14].

1.3 Scattering Characteristics of Weakly Bound Systems

Another subject widely investigated in low-energy nuclear physics is the elastic scattering of weakly bound nuclei at near-barrier energies. For tightly bound systems, the energy dependence of the phenomenological optical potential has a behavior known as the Threshold Anomaly (TA) [16,17]. It corresponds to a rapid variation of its real and imaginary parts as the energy decreases, approaching the height of the Coulomb barrier .When it happens, there is a sharp decrease of the imaginary part of the potential, owing to the closure of nonelastic channels that drains the incident flux. This drop of the imaginary part of the potential is accompanied by an increase of it real part, showing a bell-shaped energy dependence around the Coulomb barrier. This behavior is explained by the dispersion relation connecting the real and imaginary parts of the potential [18].

However, it has been shown in several works that the Threshold Anomaly (TA) is not observed in most collisions of weakly bound nuclei. In such cases, where the breakup cross section remains large even below the Coulomb barrier, the imaginary part of the potential does increase. It may even increase as the bombarding energy decreases. This increase of the imaginary part of the potential is followed by a decrease of its real part, which means that the polarization potential is repulsive [19,20]. This anomalous energy dependence of the potential was called the Breakup Threshold Anomaly (BTA) [21,22]. The BTA can be more clearly observed for neutron halo nuclei and for ^{6}Li, than for ^{7}Li [21,23,24]. Of course, the imaginary potential must decrease and eventually vanish at low enough energies. So, what actually happens is that the Coulomb barrier is no longer the proper threshold energy for such reactions. This threshold is below the barrier. It is very difficult to find experimentally where the imaginary potential vanishes, since at sub-

barrier energies the scattering is almost of fully Rutherford type .Thus, it is insensitive to the nuclear potential. However, in a few works it was possible to extrapolate the imaginary potential and find that it vanishes at energies around 85% of the height of the Coulomb barrier. This is shown in Figure (1.1) for the ^{6}Li +^{144} Sm system [25].

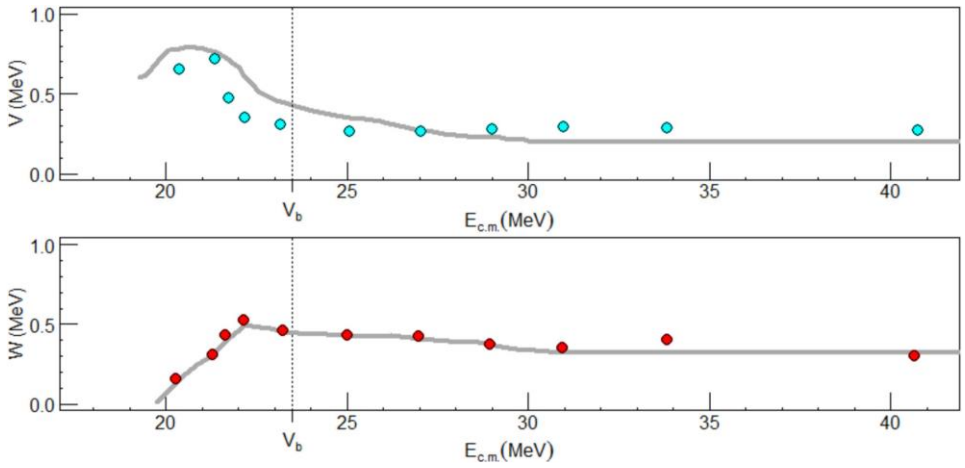

Figure 1.1 : (Color online) Energy dependence of the real and imaginary parts of the optical potential in the scattering of ^{6}Li on ^{144}Sm. Data are from [25] . The figure is adapted from [25]. The curves obey the dispersion relation [18]. The BTA [22]. can be clearly observed.

1.4 Direct Interactions

The interaction of the projectile with the outer nucleons of the target nuclei is called a direct reaction. This interaction is often occurs with one or two small energy and momentum nucleons with momentum transfer. The emission of the particle in this kind of reaction being in the direction of motion of the projectile. There is no formation of compound nucleus in the direct reaction which, generally, takes place at high energies [26]. There are many reactions can be classified as a direct reaction such as the elastic scattering, which represents the simplest form of them, where the target remains in its ground state. The situation is different in the inelastic scattering because the target will be raised to an excited state as a result of its interaction as a whole with the projectile

[27]. The Coulomb excitation of the target nucleus takes place at low incident energies, while at higher energy, the excitation becomes duo to the nuclear interaction in addition to the Coulomb excitation [28].

1.5 Halo nuclei

A motivation to study halo-nuclei systems in laboratories relies on the fact that these weakly-bound unstable nuclei, which decay naturally, have large asymmetries in the number of protons and neutrons. They are extreme cases of bound nuclei and define the neutron or proton drip line, challenging standard shell-model descriptions while privileging long range few-body correlations [29]. The study of light exotic unstable nuclei opens the possibility to go beyond the ones found in earth and look into what is created in a supernova explosion, or the nuclear mechanisms within extreme conditions allowing other cosmic events like novae . The majority of elements on earth are produced in such explosive stellar environments, involving unstable nuclei [30]. Light unstable halo-nuclei offer the opportunity to explore the many body dynamics and nuclear interaction, that bind nucleons together to form the large variety of nuclei in our universe, in the classically forbidden region: a window to truly quantum mechanical effects. Exotic nuclei with neutron excess also challenge the common understanding of traditional nuclear physics, such as the single-particle description and the associated shell structure [31,32].Nuclear halo is a spatial extension of diffuse (low density) nuclear matter significantly larger than the rest of the nucleus it envelops.

The quantum-mechanical tunneling, presented in halo nuclei, produces unexpected effects. The energy needed to remove halo nucleons is drastically less than particle separation energies for typical nuclei. Nuclear radii are enhanced but matter and charge radii may differ considerably. There is evidence that few-body effects may become

crucial, leading to the formation of cluster structures beyond the reach of mean field theories. In a first approximation, the spatial separation of particles in the halo from the rest of the system justifies a simplified description with only a few active constituents [33]. Halo nuclei can be thought of in terms of a few (typically one or two) single halo nucleons orbiting a tightly bound core, thus implying a major role of single-particle properties.

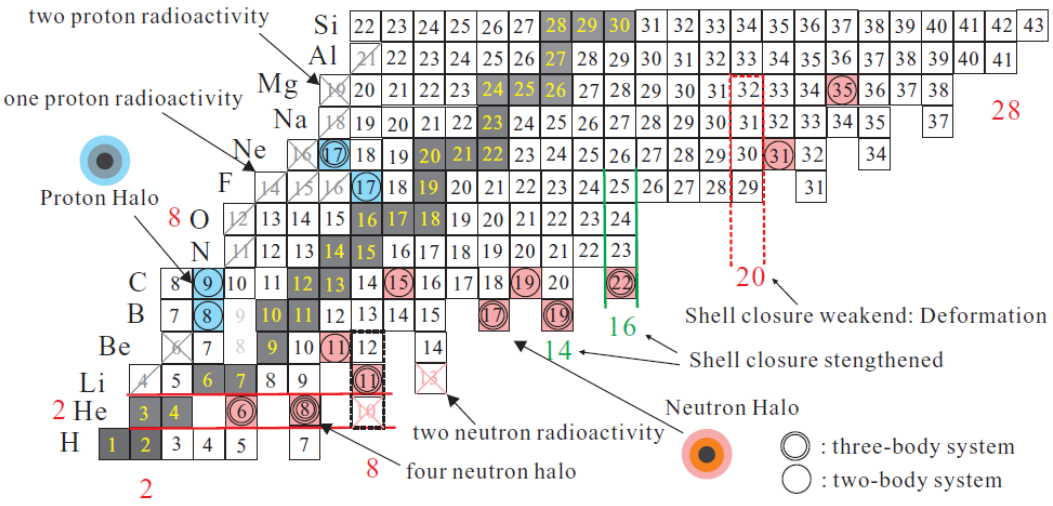

Figure 1.2 : Light exotic nuclei (halo nuclei) at the driplines of the chart of nuclides [34].

1.5.1 Neutron Halo

In experiments leading to breakup of ^{11}Li, as well as other neutron-rich nuclei, such as ^{14}Be or ^{20}C, the nuclear matter distributions near the surface can be obtained from elastic scattering or interaction cross section. The separation energy of the last two neutrons of ^{11}Li is known to be S_{2n} = 0.25 $\pm$ 0.08 MeV, while ^{10}Li is unbound [35,36]. A precise recent measurement gives S_{2n} = 369.15(65) keV, as reported in [37]. The binding energy between the two loosely bound neutrons is larger than the corresponding binding energies between each of them and the ^{9}Li core.

As argued by Hansen and Jonson [38].The strength of the neutron pairing is responsible for these differences in the separation energies [39 - 41].

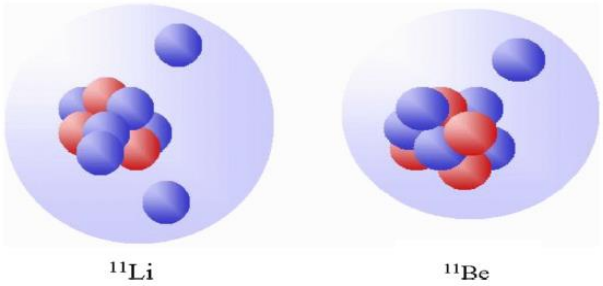

Figure 1.3 : The two best known halo nuclei are ^{11}Li with its 2-neutron halo and ^{11}Be with its single neutron halo [42].

In Figure (1.3), such diagrams should not be taken too literally as they conflate two notions: that the halo is an extended probability density distribution and at the same time the neutrons it describes are discrete particles. In a sense you can think of the former as the halo nucleus before measurement and the latter as the nucleus once the halo distribution has collapsed on measurement [42].

1.5.2 Proton halo

One might ask whether proton halos are possible. The main difference between neutrons and protons lies in the electric charge exhibited by the latter. When considering a proton weakly bound to a charged core, the long-range repulsive Coulomb potential is added to the short-ranged attractive nuclear interaction. This leads to the appearance for protons of a Coulomb barrier. It pushes the protons inside the nucleus, diminishing their probability of tunnelling outside the nuclear-interaction range. Therefore the formation of proton halos, albeit not impossible, is much less probable than that of neutron halos.

Table 1.1 Properties of proton-halo candidates. One-proton (Sp) and two-proton (Sp2) separation energy expressed in MeV [43].

Nucleus	$S_p\ (MeV)$	$S_{2p}(MeV)$
$^{8}B \equiv {}^{7}Be+p$	0.14	5.7
$^{17}F \equiv {}^{16}O+P$	0.60	12.7
$^{17}Ne \equiv {}^{15}O+2P$	1.5	0.94

The major proton-halo candidates are ^{8}B, ^{17}F, and ^{17}Ne [44]. Table 1.1 displays the one-proton (S_p) and two-proton (S_{2p}) separation energies for those nuclei. The very low S_p of ^{8}B and ^{17}F suggest that they exhibit a one-proton halo structure. ^{17}Ne exhibits a very low S_{2p}, even lower than its S_p. This might be the sign of a two-proton halo structure. However, as in the case of neutron-halo nuclei, this property is insufficient for developing a halo. Several experiments have been carried out in order to confirm the existence of proton halos. The case of ^{8}B is unclear. A measurement of its electric quadrupole moment [45]. Showed a large enhancement in comparison with that of ^{8}Li, its mirror nucleus3. This indicates a large deformation of ^{8}B, suggesting a proton-halo structure. But its interaction cross sections [46]. Do not show any significant enhancement in comparison with its neighbours. Moreover, a microscopic calculation of the ^{8}B structure [47]. Could reproduce the large electric quadrupole moment without any notion of halo. In the case of ^{17}F, it is usually admitted that its ground state does not exhibit a halo structure [48]. However, it seems that its excited state displays a halo [49].

1.6 Literature Survey

P.R.S. Gomes *et al.,* (2004) [50] implemented new measurements. and a general discussion of the behavior of the fusion, break-up and reaction cross sections of different projectiles on the same target ^{64}Zn, at near and above barrier energies. The projectiles were the tightly bound ^{16}O, the stable weakly bound ^{6}Li, ^{7}Li and ^{9}Be and the radioactive very weakly bound ^{6}He nuclei. They also compare the results with the ones for heavier targets.

P. R. S. Gomes *et al.,* (2005) [51] studied the behavior of the fusion, breakup, reaction, and elastic scattering of different projectiles on ^{64}Zn, at near and above barrier energies. They presented data on fusion and elastic scattering data with the tightly bound ^{16}O and the stable weakly bound ^{6}Li, ^{7}Li, and ^{9}Be projectiles. The data are analyzed by coupled channel calculations. The total fusion cross sections for these systems are not affected by the breakup process at energies above the barrier, the breakup process has no effect on the total fusion cross sections of these systems. At energies close to and above the Coulomb barrier, the elastic (noncapture) breakup cross section is important and increases reaction cross sections. Furthermore, They showed that the breakup process at near and below barrier energies is responsible for the disappearance of the optical potential's usual threshold anomaly and gives rise to a new type of anomaly.

M.S. Hussein *et al.,* (2006) [52] used the continuum discretized coupled channels theory takes into account the dissociation of halo nuclei caused by collisions with light and heavy targets. They looked at the one-proton halo nucleus ^{8}B, the one-neutron halo nucleus ^{11}Be, and the more common ^{7}Be. The previously used procedure for obtaining the Coulomb dissociation cross section by subtracting the nuclear one was critically examined, and the scaling law commonly assumed for the target mass

dependence of the nuclear breakup cross section is also tested. It was discovered that the nuclear breakup cross section for halo nuclei scales with target mass as $A^{1/3T}$. It does not, however, exhibit the same geometrical dependence as non-halo nuclei such as ^{7}Be. It was discovered that They can't ignore Coulomb-nuclear interference effects, which can be either constructive or destructive, and that the errors in previously extracted B(E1) using the subtraction procedure were almost certainly underestimated.

C. Beck *et al.*, (2007) [53] investigated the effect of coupling to the breakup process on fusion is for reactions in which at least one of the colliding nuclei has a low enough binding energy for breakup to become an important process. For ^{6,7}Li+^{59}Co, elastic scattering, excitation functions for sub- and near-barrier fusion cross sections, and breakup yields are investigated. The data at and above the barrier was well described by continuum-discretized coupled-channels (CDCC) calculations. Elastic scattering with ^{6}Li (rather than ^{7}Li) demonstrates the importance of breakup for weakly bound projectiles. A study of ^{4,6}He induced fusion reactions for the ^{6}He halo nucleus using a three-body CDCC method was presented. The relative importance of the effects of breakup and bound-state structure on total fusion was discussed.

David L. Canham and H.W. Hammer (2008) [54] investigated effective quantum mechanics framework, the universal properties and structure of halo nuclei composed of two neutrons (2n) and a core. They created an effective interaction potential that takes advantage of the scale separation in halo nuclei and treats the nucleus as an effective threebody system. Higher order uncertainty in the expansion is quantified using theoretical error bands. They began by looking into the possibility of observing excited Efimov states in 2n halo nuclei. According to the experimental results, ^{20}C is the only halo nucleus candidate with an

Efimov excited state with an energy less than 7 keV below the scattering threshold. They then investigated the structure of ^{20}C and other 2n halo nuclei. They calculated their matter form factors, radii, and two-neutron opening angles in particular.

Y. Kucuk and I. Boztosun (2009) [55] Displayed The elastic scattering of the halo nucleus ^{6}He from heavy targets at incident energies near the Coulomb barrier and a deviation from the standard Fresnel-type diffraction behavior. This deviation is due to the strong Coulomb dipole breakup coupling produced by the Coulomb field of the heavy target, a specific feature of the nuclear structure of ^{6}He. They have performed Continuum Discretized Coupled Channels calculations for the elastic scattering of 6He and 6Li from ^{58}Ni, ^{120}Sn, ^{144}Sm, ^{181}Ta and ^{208}Pb targets in order to determine the range of ZT where this nuclear-structure specific coupling effect becomes manifest. They found that the strong Coulomb dipole breakup coupling effect is only clearly experimentally distinguishable for targets of ZT ≈ 80.

C. Beck *et al.*, (2010) [56] Used experimental overview of reactions induced by the stable, but weakly-bound nuclei ^{6}Li, ^{7}Li and ^{9}Be, and by the exotic, halo nuclei ^{6}He, ^{8}B, ^{11}Be and ^{17}F on medium-mass targets, such as ^{58}Ni, ^{59}Co or ^{64}Zn, was presented. Existing data on elastic scattering, total reaction cross sections, fusion processes, breakup and transfer channels were discussed in the framework of a CDCC approach taking into account the breakup degree of freedom.

A.T. Rudchik *et al.*, (2010) [57] measured completed angular distributions of the ^{12}C+^{18}O elastic and inelastic scattering at the energy E_{lab}(^{18}O) = 105MeV (Ec.m. = 42MeV). Comparison of these elastic-scattering data with those from previously measured ^{12}C+^{16}O data show their large-angle cross-sections to differ by as much as a factor of 100 with the ^{16}O data being the largest. These and the ^{12}C+^{18}O scattering data

taken from the literature at the energies *E*c.m. = 12.9–56MeV were analysed within the optical model and coupled reaction- channels methods. Sets of Woods-Saxon $^{12}C + ^{18}O$ optical potential parameters were obtained and their energy dependence was deduced. A similar analysis was carried out for $^{12}C+^{16}O$ where it was shown that over a wide energy range, the primary difference in the ^{16}O and ^{18}O scattering potentials is in their imaginary parts. The large-angle enhancement for the $^{12}C+^{18}O$ elastic-scattering was shown to arise from the transfer of nucleons. The inelastic-scattering data were well described over the entire angular range as arising from collective excitations of the states in the target and projectile nuclei.

D. Naik *et al.*, (2011) [58] measured an angular distributions for the elastic scattering of ^{8}B, ^{7}Be, and ^{6}Li on a ^{12}C target at E_{lab} = 25.8, 18.8, and 12.3 MeV, respectively. The analyses of these angular distributions have been performed in terms of the optical model usingWoods-Saxon and double-folding type potentials. The effect of breakup in the elastic scattering of $^{8}B + ^{12}C$ was investigated by performing coupled-channels calculations with the continuum discretized coupled-channel method and cluster-model folding potentials. Total reaction cross sections were deduced from the elastic-scattering analysis and compared with published data on elastic scattering of other weakly and tightly bound projectiles on ^{12}C, as a function of energy. With the exception of ^{4}He and ^{16}O, the data can be described using a universal function for the reduced cross sections.

M. Cubero *et al.*, (2012) [59] presented the first measurement of the elastic scattering of the halo nucleus ^{11}Li and its core ^{9}Li on ^{208}Pb at energies near the Coulomb barrier. Even at energies well below the barrier and down to very small scattering angles, the ^{11}Li on ^{208}Pb elastic scattering shows a significant reduction in comparison to the Rutherford cross section. This dramatic change in the elastic differential cross section

observed in ^{11}Li on ^{208}Pb is due to the halo structure of ^{11}Li, as it is not observed in the elastic scattering of its core ^{9}Li at the same energies.

A.E. Woodard *et al., (*2012) [60] measured at bombarded energies close to the Coulomb barrier the angular distributions for the inelastic scattering of the weakly bound ^{6}Li nucleus from a ^{144}Sm target (associated with the contributions of both the 2_1^+ and 3_1^- ^{144}Sm excited states combined). The experimental data were compared to the predicted results using continuum discretized coupled-channel (CDCC) calculations. The findings confirm the importance of including continuum–continuum couplings in order to reproduce the experimental data. The results show that inelastic scattering data can be a valuable tool for testing full CDCC calculations involving weakly bound nuclei.

D. R. Otomar *et al.,*(2013) [61] calculated the relative importance of nuclear and Coulomb breakup on the target charge (mass) at near-barrier energies using continuum discretized coupled channel (CDCC) calculations for the ^{6}Li + ^{59}Co, ^{144}Sm, and ^{208}Pb systems. The calculations agreed well with the experimental elastic scattering angular distributions for these systems.

X. P. Yang *et al.,* (2013) [62] calculated the barrier parameters of weakly and tightly bound nuclei on different target nuclei, and the total reaction cross sections were calculated by analyzing the experimental elastic scattering data. To investigate the breakup effects, the total reaction function F(x) of weakly and tightly bound projectiles on light, medium-mass, and heavy target nuclei was systematically compared to the universal function $F_0(x)$. concluded from this comparison that the breakup effect was not important for weakly bound projectiles on light target nuclei, was suppressed on medium-mass and heavy target nuclei above the Coulomb barrier, and was enhanced for some weakly bound projectiles near and below the Coulomb barrier. More experiments for

some unstable weakly bound nuclei on medium-mass and heavy target nuclei at low energies, particularly at sub-barrier energies, were required.

N. N. Deshmukh *et al.*, (2015) [63] at various bombarding energies around the Coulomb barrier, full angular distributions for elastic and inelastic scattering of ^{11}B on ^{58}Ni have been measured. For the first time, coupled-channel calculations were used to measure and analyze a system with a tightly bound ^{11}B projectile on a medium mass target. The real part of the interaction potential between nuclei was represented in these calculations by a parameter-free double-folding potential. To avoid the use of an imaginary potential at the surface, the coupling matrix includes several inelastic transitions of the projectile and the target. All experimental angular distributions agree very well with the results of these coupled-channel calculations.

Kosho Minomo *et al.*, (2016) [64] investigated the coupled-channels and three-nucleon-force (3NF) effects on elastic and inelastic cross sections using the microscopic coupled-channels method. The Melbourne g-matrix interaction, modified according to the chiral 3NF effects, is used in the microscopic coupled-channels calculation. It is discovered that the coupled-channels and 3NF effects change both the elastic and inelastic cross sections additively. As a result, the coupled-channels calculation with 3NF effects improves the agreement between theoretical and experimental results significantly. The incident-energy dependence of coupled-channels and the 3NF effects are also discussed.

Y. Y. Yang *et al.*, (2016) [65] the elastic scattering cross sections of the neutron-rich nucleus ^{11}Be were greatly reduced by the coupling effects of the breakup channels, but not those of the proton-rich nucleus ^{8}B. The continuum-discretized coupled channel (CDCC) method was used to calculate 8B elastic scattering from ^{208}Pb at 60 and 170.3 MeV and ^{64}Zn at 32 and 86 MeV, as well as ^{11}Be elastic scattering from ^{208}Pb

at 55 and 143 MeV and ^{64}Zn at 29 and 66 MeV. The Coulomb and centrifugal barriers encountered by the valence proton in the ground state of ^{8}B, which do not exist for the valence neutron in the ground state of ^{11}Be, were discovered to be the cause of such differences in the angular distributions of elastic scattering cross sections of these two weakly bound nuclei.

V. Scarduelli *et al.*, (2017) [66] measured at various energies around the Coulomb barrier, the full angular distributions of the ^{10}B elastically and inelastic scattered by ^{58}Ni. For the first time, the elastic and inelastic scattering of ^{10}B on a medium mass target has been measured. The obtained angular distributions were analyzed in terms of large-scale coupled reaction channel calculations, in which the coupling matrix included several inelastic transitions of the projectile and the target, as well as the most relevant one- and two-step transfer reactions. The roles of spin reorientation, spin-orbit interaction, and spin-orbit interaction, In the reaction mechanism, the large ground-state deformation of the ^{10}B was also investigated. A parameter-free double-folding potential was used to represent the real part of the interaction potential between projectile and target, while no imaginary potential at the surface was considered. In this sense, the theoretical calculations were parameter-free, and the results were compared to experimental data to determine the relative importance of the various reaction channels. The ground-state spin reorientation of the ^{10}B nucleus had a significant influence on the system's dynamics, while all transfer reactions investigated had a negligible contribution to the system's dynamics. Finally, the large static deformation of the ^{10}B as well as the spin-orbit coupling can both play important roles in the system under consideration.

B.V.Carlson *et al.*, (2017) [67] used a four-body spectator model to discuss the inclusive breakup of three-fragment projectiles. In a unified

framework, both the elastic and non-elastic breakups were obtained. Originally developed in the 1980s for two-fragment projectiles like the deuteron, the theory was successfully generalized to three-fragment projectiles in this paper. The inclusive cross section expression obtained allows the extraction of the incomplete fusion cross section, and thus generalizes the surrogate method to cases such as (t,p) and (t, n) reactions. It was discovered that two-fragment correlations within the projectile have a noticeable effect on the elastic breakup cross section. The inclusive non-elastic breakup cross section is calculated and found to contain a three-body absorption term that was also strongly influenced by the two-fragment correlations. This latter cross section contains what was known as incomplete fusion, which occurs when more than one compound nuclei were formed. Both stable weakly bound three-fragment projectiles and unstable ones, such as the Borromean nuclei, were described in their theory.

Rodrigo Navarro Pérez and Jin Lei (2019) [68] demonstrated the first rigorous uncertainty quantification on elastic nucleus nucleus scattering at energies close to the Coulomb barrier. The experimental data was analyzed by employing an energy-dependent effective optical model potential with physical constraints. They confirmed the compatibility of these uncertainties with the well-known Coulomb threshold anomaly, which they explained in terms of a dispersive relation, and compared their findings to previous analyses that suggested otherwise.

L. M. Fonseca *et al.*, (2019) [69] when the relevant couplings are included in the calculations, nuclear scattering at energies well above the Coulomb barrier allows for a fairly sensitive examination of the optical potential parameters. They presented experimental data for the elastic and inelastic scatterings of ^{16}O impinging on ^{27}Al and ^{28}Si target nuclei at E_{lab} = 240 MeV. The experimental data were collected at $7^\circ < \theta_{c.m.} < 16^\circ$.

with high angular resolution. The experimental data was compared to coupled channel calculations that include couplings to excited states in the target and projectile. They demonstrate that the shape of angular distributions is sensitive to the mass diffuseness parameter, with a = 0.62 fm providing the best agreement.

Ashjan J. Hassan and Khalid S. Jassim (2020) [70] the nuclear potential Woods-Saxon (WS) method was used to investigate the effects of surface diffuseness parameter on quasi-elastic scattering for ^{6}He+^{64}Zn, ^{7}Li+^{64}Zn, and ^{8}Li+^{90}Zr systems. For the nuclei ^{64}Zn with ground state rotational band up to the 4+ states, the effect of rotational deformation was included. They performed single (SC) and coupled-channels (CC) calculations to obtain the best compatibility between the notional accounts of d_{qel}/d_R and experimental data for the systems under consideration. They discover that the best-fitting value of the diffuseness parameter obtained using a coupled-channel calculation with an inert target and an excited projectile In the current study, the single-channel (SC) and coupled-channel (CC) calculations, which were between the relative motion of colliding nuclei and their intrinsic motions, were performed to study its influence on calculation, the ratio of the quasi-elastic to the Rutherford cross sections, and probe the surface diffuseness find that the best fitted value of the diffuseness parameter which obtained through a coupled- channel calculation with inert target and excited projectile for the ^{6}He+^{64}Zn, ^{7}Li+^{64}Zn and ^{8}Li+^{90}Zr.

1.7 Aim of the present work

The aim of the thesis is to employ a full quantum mechanic in study the effect of coupling channels with breakup channel on systems invlo **^{6}He + ^{120}Sn**, **^{6}Li + ^{64}Zn**, **^{7}Li + ^{64}Zn**, **^{8}B + ^{58}Ni**, **^{9}Be + ^{64}Zn**, **^{12}C + ^{208}Pb**, **^{6}He+^{58}Ni**, and **^{11}Be+^{197}Au**, to calculation the total (elastic and inelastic) scattering cross sections and the distribution of the barrier. And

the comparison between the theoretical results with the corresponding experimental data.

Chapter Two

Theoretical part

2.1 Introduction

The most important experimental technique in quantum physics is the scattering experiment, where in nuclear physics, the first clear evidence of nuclear structure came from Rutherford's observation of the scattering reaction. The theoretical tool for the analysis of scattering experiments is scattering theory, which is used to study of an interacting system on a large time and/or distance scale compared to the actual interaction scale [71, 72]. In general, the results of a nuclear collision may be one of many possible reactions, each one of which sheds light on a particular aspect of nuclear structure or nuclear behavior. Research scientists measure different reactions to study the nuclear force, synthesize new nuclei, determine nuclear size and shapes, and investigate the properties of excited nuclei. According to the conventional view, depending on the impact parameter or the corresponding angular momentum, the projectile can cause a variety of reactions. and the dynamical behavior of nuclear matter during different types of collision in the classical picture of heavy ion (HI) as shown in Figure (2.1) [73,74,75].

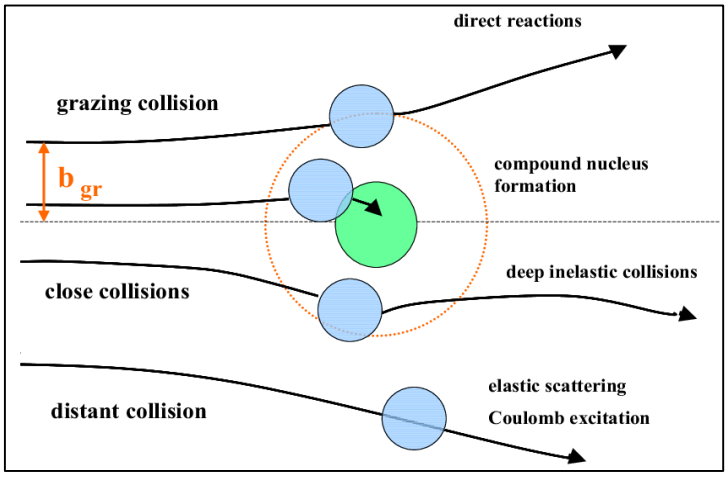

Figure 2.1: In the classic picture of heavy ion collisions, there are distant, grazing, and close collisions. adapted from [76].

2.2 Types of scattering reactions

2.2.1 Elastic Scattering

In an elastic scattering event, the nucleus of the target remains in the ground state after the scattering. Using the same notation as before, elastic scattering can be described as A(n,n)A Figure (2.2) which illustrates the elastic scattering of a neutron on a nucleus in both the laboratory system (L) and the centre of mass system (CM). The two different coordinate systems describe the process of elastic scattering from two different point of views. The L-system proceeds from the perspective of a coordinate system in rest relative to a spectator. In contrast, the CM-system is a coordinate system in motion, following the centre of mass of the system. Various velocity components and scattering angles are indicated in Figure (2.2). In the L-system, a neutron with a velocity of v_{n0} collides with a nucleus approximated as being at rest initially. Such an approximation is not valid around thermal energies, since the speeds of the neutron and the nucleus then are relatively similar [77]. The velocity of the neutron after the collision is vn1 and its scattering angle. The transformation of the velocity of the neutron from the L-system to the CM-system is given in Equation (2.1). Also of importance for the scope of this thesis is the velocity of the CM-system given in Equation (2.2). Since the velocity of the nucleus is zero in the L-system, Equation (2.2) also represents the velocity of the nucleus in the CM-system. The masses of the nuclei have been normalised to the mass of the neutron, giving that the mass of the particle corresponds to the atomic mass number (A) [78,79].

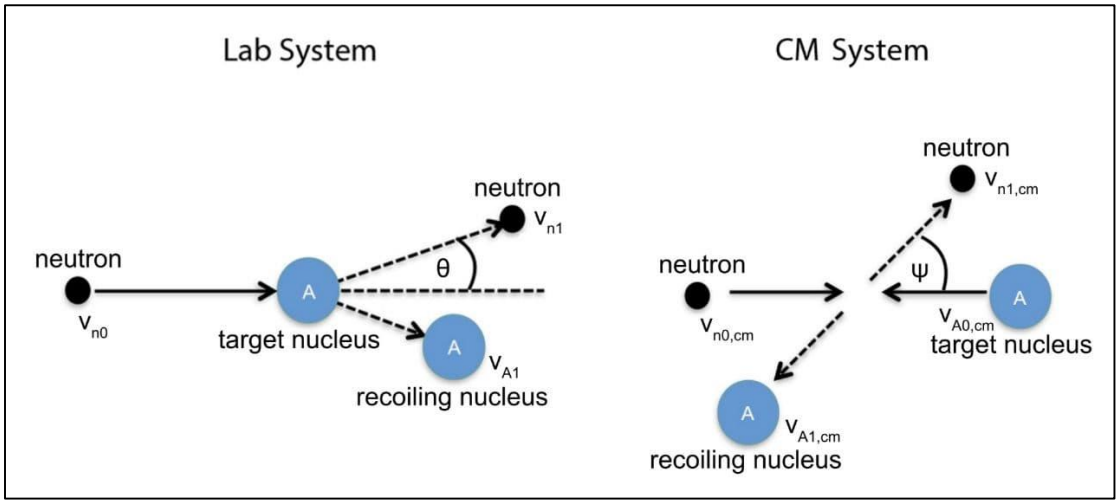

Figure 2.2: Illustration of the elastic scattering of a neutron on a target nucleus, A. The scattering event is described both in the laboratory system (left) and the centre of mass system (right) [80].

$$\upsilon_{n0,cm} = \frac{A}{A+1}\upsilon_{n0} \tag{2.1}$$

$$\upsilon_{cm} = \frac{1}{A+1}\upsilon_{n0} \tag{2.2}$$

The benefit of transforming the parameters of the L-system to the CM-system can be seen from analysing the precollision parameters. If the momentum of the particles before collision is considered in the CM-system, it is evident that the total momentum in this system equals zero. Since elastic scattering is considered, the total momentum will be conserved after the collision and, as a result, also the speed. After the collision, the trajectory of the neutron changes with an angle in the CM-system [79,81]. Figure (2.3) represents a summary of two post-collision velocity vectors related to the CM system. The horizontal vector represents the velocity of the moving coordinate system (v_{cm}), and the far right vector represents the neutron velocity. As shown, adding these vectors yields the neutron's post-impact velocity in the L-system (v_{n1}).

This velocity can be expressed using the law of cosines as in Equation (2.3),

$$v_{n1}^2 = (\frac{v_{n0}}{A+1})^2 + (\frac{v_{n0}A}{A+1})^2 + 2\frac{v_{n0}}{A+1}\frac{v_{n0}A}{A+1}\cos(\psi), \quad (2.3)$$

where the angle θ is proportional to ψ according to Equation (2.4) [79].

$$\cos\theta = \frac{A\cos\psi+1}{\sqrt{A^2+1+2A\cos\psi}} \quad (2.4)$$

By utilising the relationship between kinetic energy and velocity, Equation (2.5) gives the relative.

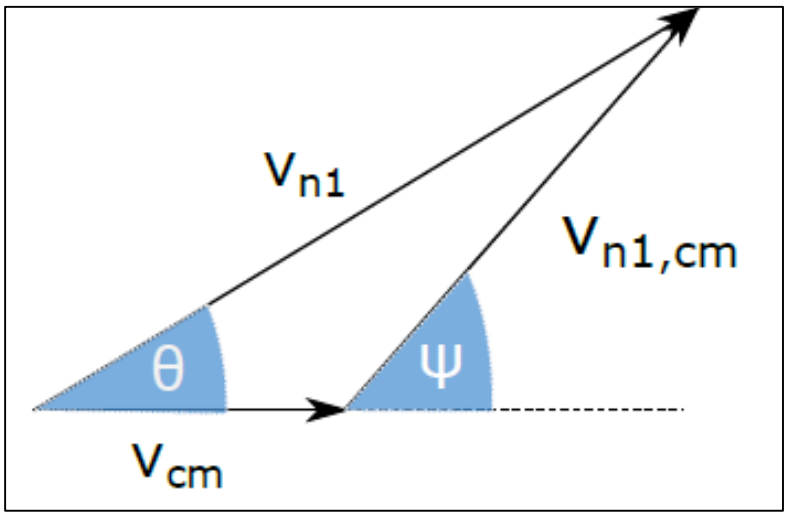

Figure 2.3: The sum of two velocity vectors from the CM-system, that of the moving coordinate system and that of the scattered neutron, is depicted schematically [81].

The neutron's energy is defined as the ratio of its post-collision kinetic energy (E_{n1}) to its original energy (E_{n0}).

$$\frac{E_{n1}}{E_{n0}} = \frac{2A\,cos\,\psi + A^2 + 1}{(A+1)^2} \quad (2.5)$$

While $\psi = \pi$, i.e. when the neutron is backscattered in the CM-system, the energy of the scattered neutron is at a minimum. The corresponding angle in the L-system can be found from Equation (2.4) The largest value occurs for ψ

=0, i.e. for forward scattering. Thus, the range of the neutron energy after scattering is:

$$\left(\frac{A-1}{A+1}\right)^2 E_{n0} < E < E_{n0} \quad (2.6)$$

The target nucleus, according to Equation (2.6), indicates that the target nucleus will have a profound effect on the range of the post-collision energy of the neutron. Evidently, moderation will be most effective if lighter nuclei are used.

2.2.2 Inelastic scattering

Inelastic scattering is the phenomena where the target nucleus is left in an excited state after the scattering event. In the shorted notation, inelastic scattering is written A(n,n)A*, where the star indicates that the initial nucleus has entered an excited state. Since a certain amount of energy is needed to excite a nucleus, E_{exc}, inelastic scattering is only possible if the kinetic energy of the neutron is above a certain threshold. The relative kinetic energy of the neutron after scattering can be derived in a similar way as Equation (2.5). The result is stated in Equation (2.7).

$$\frac{E_{n1}}{E_{n0}} = \frac{\gamma^2 + 1 + 2\gamma\cos(\psi)}{(A+1)^2} \quad (2.7)$$

where $\gamma = \left(A\sqrt{1-(A+1/A)\,E_{exc}/E_{n0}}\right)$. If the excitation energy is zero, Equation (2.7) is reduced to the case of elastic scattering in Equation (2.5) [79]. According to the previous analogy about elastic scattering, as well as Equation (2.6), neutrons that are elastically scattered in heavier material only lose a small fraction of their initial energy in each collision. As a result, inelastic scattering will be more important in moderators made up of heavier elements [78].

2.3 Rutherford scattering

2.3.1 Classical-mechanical derivation of Rutherford's formula

On the other hand, using a model based on classical trajectories, one might conceive Coulomb scattering [82]. In fact, semiclassical or classical approximations are frequently enough for describing elastic scattering processes. This is especially true for experiments using heavy ion scattering. Because the Coulomb barrier for heavy projectiles is so large, calculations on the peak of the Coulomb-wall (V_C) with the projectile's reduced kinetic energy are required: $E = E_{cm} - V_C$ [84]. The differential cross section for the elastic scattering of a charged particle by an electrostatic potential generated by a point charge is calculated using a classical derivation. Rutherford scattering is another name for this phenomenon. In Figure (2.4), a particle is shown being deflected through an angle θ by a scattering center of charge (Z_T e). the particle has charge (Z_P e), mass m, speed v, impact parameter b and energy $E = \frac{1}{2}mv^2$. We assume, for simplicity, that the scatterer remains at rest that is, we shall take the scatterer to be infinitely heavy. The angle of the position vector r to the z-axis is ϕ and we can use conservation of angular momentum to write [83].

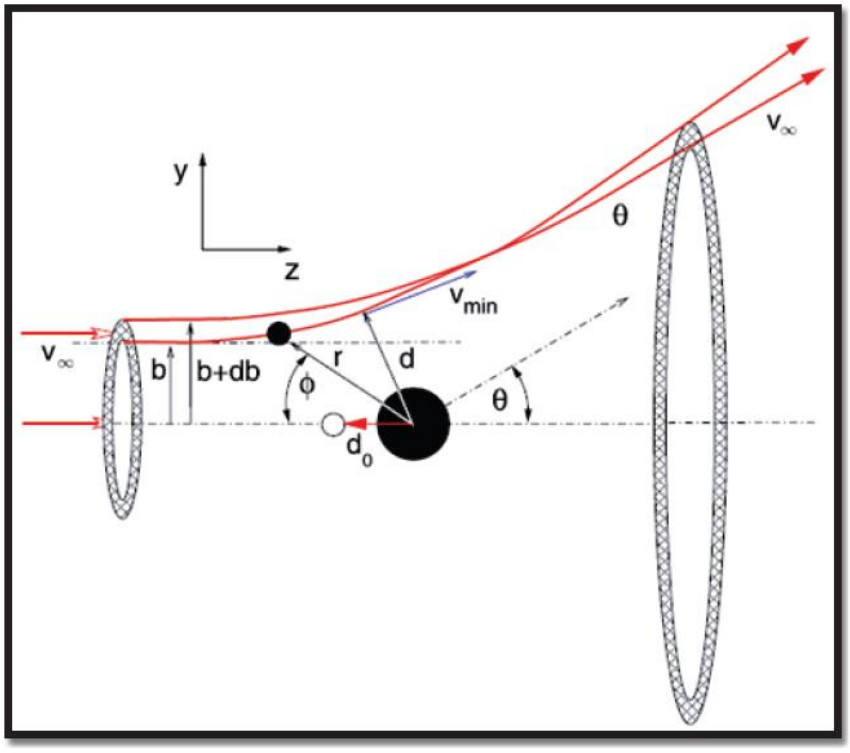

Figure 2.4: Classical Rutherford scattering. *b* is the impact parameter, (*r*,ϕ) are the polar coordinates of the projectile, θ the polar scattering angle, *d* is the distance of closest approach, and d_0 its minimum for a central collision [83].

$$L = mv_{\infty}b = mr^2\frac{d\emptyset}{dt} = mv_{min}d \tag{2.8}$$

We can also calculate $\Delta p = m\Delta v_y$ as the integral over the trajectory of the *y* component of the impulse on the particle due to the Coulomb force F_C acting on it, as following [84, 85].

$$F_C = \pm\frac{1}{4\pi\varepsilon_0}.\frac{Z_P Z_T e^2}{r^2} = \pm\frac{C}{r^2} \tag{2.9}$$

Where,

$$C = \frac{Z_P Z_T e^2}{4\pi\varepsilon_0} \tag{2.10}$$

$$dt = \frac{r^2 d\emptyset}{v_{\infty}b} \tag{2.11}$$

$$\Delta p = \int F_C \, dt \tag{2.12}$$

$$v_\infty \sin\theta = \frac{C}{m v_\infty b} \int_{-\infty}^{\infty} \sin\emptyset \frac{d\emptyset}{dt} dt \tag{2.13}$$

$$\frac{C}{m v_\infty b} \int_0^{\pi-\theta} \sin\emptyset \mathrm{d}\emptyset = \frac{\mathrm{C}}{\mathrm{m}\upsilon_\infty \mathrm{b}} (1 + \cos\theta) \tag{2.14}$$

The deflection function is transformed to half the scattering angle.

$$\cot(\theta/2) = \frac{m v_\infty^2 b}{C} = \frac{v_\infty L}{C} \tag{2.15}$$

and

$$b = \frac{C}{2E_\infty} . \cot(\frac{\theta}{2}) \tag{2.16}$$

the derivative of Eq.(2.16) is [84, 83, 85, 82].

$$\frac{db}{d\theta} = \frac{C}{m v_\infty^2} . \frac{1}{sin^2\left(\frac{\theta}{2}\right)} = \frac{C}{4E_\infty} . \frac{1}{sin^2\left(\frac{\theta}{2}\right)} \tag{2.17}$$

and thus for the Rutherford differential cross section [83].

$$\frac{d\sigma}{d\Omega} = \left[\frac{Z_P Z_T e^2}{4E_\infty}\right]^2 \frac{1}{sin^4\left(\frac{\theta}{2}\right)} \tag{2.18}$$

Numerically [86].

$$\frac{d\sigma}{d\Omega} = 1.296(\frac{Z_P Z_T e^2}{E_\infty (MeV)})^2 . \frac{1}{sin^4\left(\frac{\theta}{2}\right)} \left[\frac{mb}{sr}\right] \tag{2.19}$$

The energy-conservation law is also required for determining the minimal scattering distance *d* [83, 85].

$$\frac{m v_\infty^2}{2} = \frac{m v_{min}^2}{2} + \frac{C}{d} \tag{2.20}$$

In central collisions with, the absolute smallest distance d_0 is obtained. [83].

$$E_\infty = \frac{C}{d_0} \tag{2.21}$$

The relationship is deduced from this and the angular-momentum conservation [83, 85].

$$b^2 = d(d - d_0) \tag{2.22}$$

is obtained with the solution [83].

$$d = \frac{C}{2E_\infty}\left(1 + \sqrt{1 + b^2\frac{4E_\infty^2}{C^2}}\right) = \frac{d_0}{2}\left(1 + \frac{1}{\sin(\theta/2)}\right) \tag{2.23}$$

2.3.2 Quantum-mechanical Derivation of Rutherford's Formula

The Schrödinger equation describes the scattering of one particle off another in the nonrelativistic limit. The wave function in the CM is the solution to the equation [86, 87].

$$-\frac{\hbar^2}{2\mu}\nabla^2\psi + (V - E)\psi = 0 \tag{2.24}$$

where μ denotes the reduced mass in the two-nucleon system and V denotes the central potential. A spherical wave $\frac{e^{ikr}}{r}$ radiating outward from the center of the interaction region describes the scattered particle outside the interaction region. The particle density in the incident beam is usually low enough that any interference between incident and scattering particles can be ignored. As a result, at large r, the wave function is a linear combination of a plane wave (the incident beam and particles not scattered by the potential) and a spherical wave (scattered particles). The outcome can be expressed as [87-90].

$$\psi(\vec{r}) \underset{r\to\infty}{\longrightarrow} e^{ikz} + f(\theta, \emptyset)\frac{e^{ikr}}{r} \tag{2.25}$$

In this case, $f(\theta, \emptyset)$ is the scattering amplitude, which measures the fraction of the incident wave scattered in the direction with the polar angle and azimuthal angle. In general, $\psi(\vec{r})$ and $f(\theta, \emptyset)$ are both functions of the incident wave vector k and the scattered wave vector k. Furthermore, the probability of scattering is low enough that particles removed from the incident beam due to scattering have no effect on the normalization of the incident wave. The zy-plane is fixed by requiring it to be perpendicular to the z-axis because the z-axis is chosen to be along the direction the two particles approaching each other outside the interaction zone [87, 89].

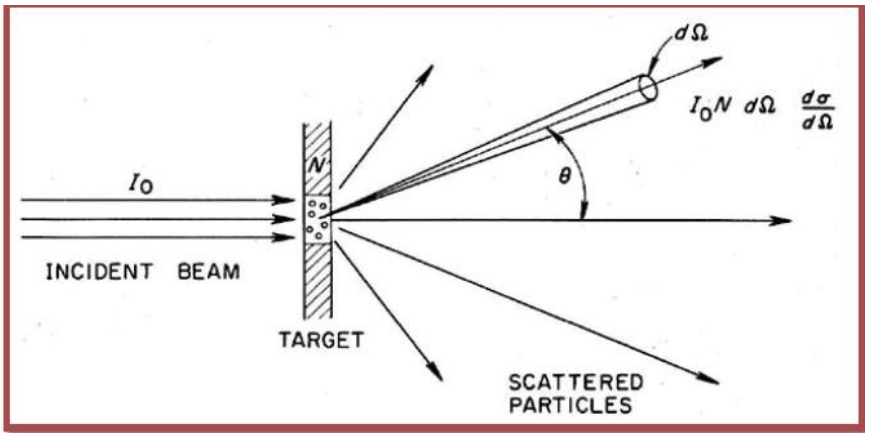

Figure 2.5: Diagram for the definition of differential cross-section [85].

From Figure (2.5), the relation between wave function and intensity of the incident beam is given by the quantum-mechanical probability current density [86, 91].

$$\vec{j_i} = \frac{\hbar^2}{2i\mu}\left[\psi^* \vec{\nabla}\, \psi - \ \psi \vec{\nabla}\, \psi^*\ \right] = Re\left\{\psi^* \frac{\hbar}{i\mu} \vec{\nabla}\, \psi\right\} \tag{2.26}$$

$$j_i = Re\left\{e^{-ikz}\ \frac{\hbar}{i\mu}\frac{d}{dz}\ e^{ikz}\right\} = \frac{\hbar k}{\mu} \tag{2.27}$$

where *Re* stands for the real part. The differential scattering cross section may be expressed in terms of the scattering amplitude $f(\theta)$. The probability current density for the scattered spherical wave is given by the expression [72,92].

$$\vec{J}_{sc} = R_e\left\{\left(f(\theta)\frac{e^{ikr}}{r}\right)^{*}\frac{\hbar}{i\mu}\frac{d}{dr}\left(f(\theta)\frac{e^{ikr}}{r}\right)\right\} = \vec{J_i}\frac{|f(\theta)|^2}{r^2}\hat{r} \tag{2.28}$$

When a scattered particle is observed by a detector with an effective area dA placed at r from the scattering center, the solid angle subtended by the detector at the origin is [93].

$$d\Omega = \frac{dA}{r^2} \tag{2.29}$$

as well as the number of particles recorded per unit of time [87].

$$N_{sc} = \vec{J}_{sc}\, dA = \vec{J}_{sc}\, r^2 d\Omega \tag{2.30}$$

And

$$N_i = \frac{\hbar k}{\mu} d\Omega \tag{2.31}$$

The differential scattering cross section, $\frac{d\sigma}{d\Omega}$ is defined as the number of particles scattered into a solid angle $d\Omega$ at angle divided by the incident flux, [89, 94].

$$\frac{d\sigma}{d\Omega} = \frac{\vec{J}_{sc}\, r^2}{\vec{J}_i} = |\, f(\theta)|^2 \tag{2.32}$$

The scattering cross section is defined as the integral of the differential cross section across all solid angles [95].

$$\sigma = \int \frac{d\sigma}{d\Omega} d\Omega = 2\pi \int_0^{\pi} |f(\theta)|^2 \sin\theta \, d\theta \tag{2.33}$$

where

$$d\Omega = \sin\theta \, d\theta \, d\phi \tag{2.34}$$

If the interaction potential is central, V = V(r), and depends only on the relative distance r, angular momentum is a constant of motion. In this case, decomposing the wave function ψ (r) into a product of radial and angular parts and writing it as a sum over components with definite orbital angular momentum l, or partial waves, is convenient [83, 87].

$$\psi(r,\theta) = \sum_{l=0}^{\infty} a_l \, R_l \, (r) Y_{l0}(\theta) \tag{2.35}$$

where a_l are the expansion coefficients. Only spherical harmonics $Y_{\mathrm{lm}}(\theta,\phi)$with m = 0 are involved in this case, because we are looking at systems that are independent of the azimuthal angle ϕ in terms of the modified radial wave function [91].

$$u_l \, (r) = r \, R_l(r) \tag{2.36}$$

The equation simplified of differential equation [90, 91].

$$\frac{d^2 u_l \, (r)}{dr^2} - \left\{ \frac{l(l+1)}{r^2} + \frac{2\mu}{\hbar 2} V(r) - k^2 \right\} u_l \, (r) = 0 \tag{2.37}$$

For short-range potentials, V(r) approaches zero as $r \longrightarrow \infty$ decreases. The same is true for the $\frac{l(l+1)}{r^2}$ term. In the asymptotic regions, we are left with a simple second-order differential equation differential equation of the form [89, 90].

$$\frac{d^2u_l(r)}{dr^2} + k^2u_l(r) = 0 \tag{2.38}$$

The solution of this equation is the well-known linear combination of $sin(kr)$ and $cos(kr)$. In other words, at large r, the function $u_l(r)$ must take the form [87, 90, 93].

$$u_l(r) \xrightarrow[r\to\infty]{} A_l \sin(kr - \frac{1}{2}l\pi) + B_l \cos(kr - \frac{1}{2}l\pi)$$

$$= C_l \sin(kr - \frac{1}{2}l\pi + \delta_l) = C_l' \left\{ e^{-i(kr-\frac{1}{2}l\pi)} - e^{2i\delta_l} e^{i(kr-\frac{1}{2}l\pi)} \right\} \tag{2.39}$$

where A_l and B_l, or C_l (C_l'), are two constants that must be calculated based on boundary conditions, and δ_l is the phase shift. The phase factor $\frac{1}{2}l\pi$ is included here to make comparisons with the asymptotic form of spherical Bessel functions easier. By comparing Eq.(2.40) to the partial wave expansion of a plane wave, we can see its physical meaning [91, 95].

$$e^{ikz} = \sum_{l=0}^{\infty} \sqrt{4\pi(2l+1)}\; i^l j_l(kr) Y_{l0}(\theta) \tag{2.40}$$

The spherical Bessel function $j_l(kr)$ has the form asymptotically [96].

$$j_l(kr) \xrightarrow[r\to\infty]{} \frac{\sin(kr - \frac{1}{2}l\pi)}{kr} \tag{2.41}$$

Compared with that of Eq.(2.40). A plane wave in the asymptotic region can be written as [85, 90].

$$e^{ikz} \xrightarrow[r\to\infty]{} \sum_{l=0}^{\infty} \sqrt{4\pi(2l+1)}\; \frac{i^l}{kr} \sin(kr - \frac{1}{2}l\pi) Y_{l0}(\theta)$$

$$= \sum_{l=0}^{\infty} \sqrt{4\pi(2l+1)} \left\{ \frac{e^{ikr}}{2ikr} - \frac{i^l e^{-i(kr-\frac{1}{2}l\pi)}}{2ikr} \right\} Y_{l0}(\theta) \qquad (2.42)$$

The asymptotic form of the wave function given earlier in Eq.(2.35), we arrive at the equality [87, 90].

$$e^{ikz} + f(\theta)\frac{e^{ikr}}{r} = \sum_{l=0}^{\infty} \acute{a}_l Y_{l0}(\theta) \frac{1}{r} \sin(\, kr - \frac{1}{2} l\pi + \delta_l)$$

$$= \sum_{l=0}^{\infty} \acute{a}_l Y_{l0}(\theta) \left\{ (-i)^l e^{i\delta_l} \frac{e^{ikr}}{2ikr} - e^{-i\delta_l} \frac{e^{-i(kr-\frac{1}{2}l\pi)}}{2ikr} \right\} \qquad (2.43)$$

Where $\acute{a}_l = \sqrt{4\pi(2l+1)}\, i^l e^{i\delta_l}$, In terms of phase shifts, the scattering amplitude can be written as,

$$f(\theta) = \frac{\sqrt{4\pi}}{k} \sum_{l=0}^{\infty} \sqrt{(2l+1)}\ e^{i\delta_l} \sin\delta_l Y_{l0}(\theta) \qquad (2.44)$$

The differential scattering cross section can be written as [87, 91].

$$\frac{d\sigma}{d\Omega} = \frac{4\pi}{k^2} \left| \sum_{l=0}^{\infty} \sqrt{(2l+1)}\ e^{i\delta_l}\ \sin\delta_l Y_{l0}(\theta) \right|^2 \qquad (2.45)$$

From the orthogonal condition on spherical harmonics [87].

$$\int_0^{2\pi} \int_0^{\pi} Y_{lm}^*(\theta, \emptyset) Y_{\acute{l}\acute{m}}(\theta, \emptyset) \sin\theta\, d\theta\, d\emptyset = \delta_{l\acute{l}} \delta_{m\acute{m}} \qquad (2.46)$$

The scattering cross section can be simplified to a very simple form. at $l = \acute{l}$ [92, 87, 94].

$$\sigma_{sc} = \frac{4\pi}{k^2}\sum_{l\acute{l}}\sqrt{(2l+1)\left(2\acute{l}+1\right)}\; e^{i(\delta_l-\delta_{\acute{l}})}\sin\delta_l\sin\delta_{\acute{l}}\int_0^{\pi} Y_{l0}(\theta)Y_{\acute{l}0}(\theta)\sin\theta d\theta$$

$$= \frac{4\pi}{k^2}\sum_{l=0}^{\infty}(2l+1)\sin^2\delta_l \qquad (2.47)$$

For this case, $4\sin^2\delta_l = |1-\eta_l|^2$, and η_l is reflection coefficient.

$$\sigma_{sc} = \frac{\pi}{k^2}\sum_l(2l+1)\,|1-\eta_l|^2 \qquad (2.48)$$

Only elastic scattering can take place. Where $4\sin^2\delta_l = |1-\eta_l|^2$, $|\eta_l| = 1$.

2.4 Nuclear potential

The nucleus-nucleus potential consists of two parts: The first is the nuclear part V_N which can be described well and fairly reasonably by the Wood-Saxon form which is given by:

$$V_N(r) = -\frac{V_0}{1+exp\left[\frac{r-R_0}{a}\right]} \qquad (2.49)$$

Where $R_0 = r_0(A_T^{\frac{1}{3}} + A_P^{\frac{1}{3}})$, R_0 is a radius of the system.

where V_0, a and r_0 represent the potential depth, surface diffuseness parameter, and radius parameter, respectively whilst r refers to the center of mass distance between the target nucleus of mass number A_T and the projectile nucleus of mass number A_P [97,98].

The diffuseness parameter described the property at the surface area of the nuclear potential, where Figure (2.6) show the property of the nuclear potential V_N at the surface region as a function of the distance between the projectile and the target to the system $^{32}S+^{208}Pb$ for example, where the largest diffuseness parameter a =1 fm (represented by the dashed line) makes the nuclear potential become more spread out.

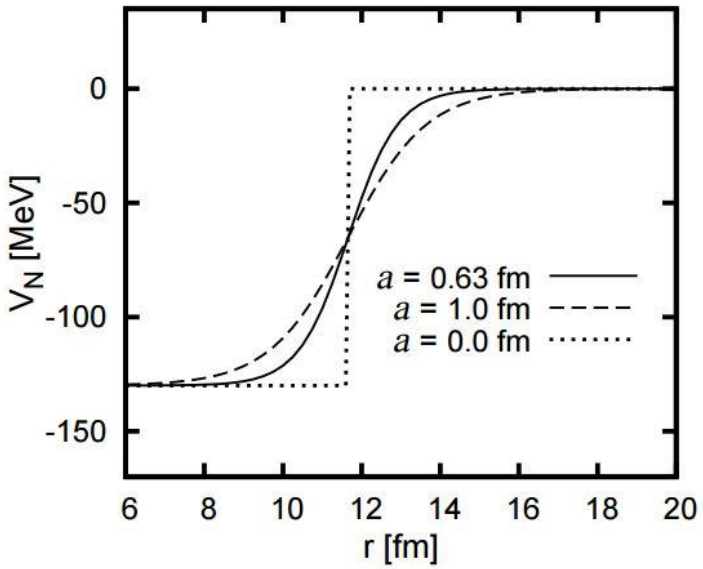

Figure 2.6: Shows the property of the nuclear potential V_N at the surface region as a function of the distance between the projectile and the target to the system $^{32}S+^{208}Pb$ using three different values of the diffuseness parameter [99].

On the other hand, the second part is a Coulomb part $V_C(r)$ between two spherical nuclei with regular charge density distributions, when they do not interfere, is given by [99,100]:

$$V_c(r) = \frac{Z_P Z_T e^2}{4\pi\varepsilon_0 r}, \qquad r > R_c \qquad (2.50)$$

where Z_p and Z_T represent the atomic number of the projectile and target respectively, r is the distance between the center of mass of the colliding nuclei . R_c is the radius of the ball equivalent to the nuclei of the target and the projectile where $R_c = r_c(A_T^{\frac{1}{3}} + A_P^{\frac{1}{3}})$, r_c is a Coulomb radius parameter [99]. When the nuclei interfere, then the Coulomb potential is given by [99,100].

$$V_c(r) = \frac{Z_P Z_T \ e^2}{8\pi\varepsilon_0 R_C}\left[3 - \left(\frac{r}{R_C}\right)^2\right] \qquad r \leq R_C \qquad (2.51)$$

A potential between the projectile and the target is given by a function of the relative distance r between the center of mass of the colliding nuclei. It consists of two parts given by [98].

$$V(r) = V_N(r) + V_c(r) \tag{2.52}$$

The radial Schrödinger equation comprises an effective potential, which defined by the following equation [101].

$$V_{eff}(l,r) = V_N(r) + V_C(r) + \frac{\hbar^2 l(l+1)}{2\mu r^2} \tag{2.53}$$

Effective potential is the sum of nuclear, Coulomb and centrifugal components. When angular momentum l = 0, the compound centrifugal vanish. Figure (2.7) clears inter-nucleus potential between ^{16}O and ^{154}Sm nuclei as a function of the relative distance. Nucleus-nucleus interaction for ^{16}O+^{154}Sm system at zero angular momentum is l = 0. The nucleus-nucleus potential produces a Coulomb barrier height V_b, situated at a distance R_b between the centers of the colliding nuclei.

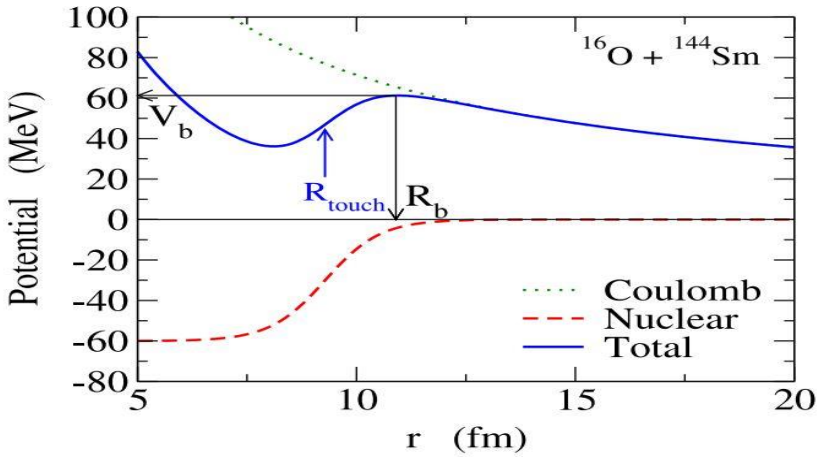

Figure 2.7: This diagram depicts the typical nucleus-nucleus interaction for the ^{16}O+^{144}Sm heavy-ion system with zero angular momentum l = 0. Coulomb potential $V_C(r)$, Nuclear potential $V_N(r)$, and the sum of $V_N(r)$ and $V_C(r)$ are represented by the dotted, dashed, and solid lines, respectively [98].

2.5 Continuum discretized coupled channel formalism

Consider the reaction described by the total wave function $\Psi(\vec{r},\tau)$, where r stands for the projectile and target nuclei separation vector and τ for the set of intrinsic coordinates of the projectile and target nuclei. The dynamics of this reaction is determined by the Hamiltonian,

$$H = H_0 + T + U \tag{2.54}$$

where $H_0 \equiv H_0(\tau, p_\tau)$ is the intrinsic Hamiltonian, $T \equiv -\hbar^2 \boldsymbol{\nabla}^2/2\mu$ is the kinetic energy operator of the relative motion between the projectile and target nuclei, and $U \equiv U(\mathbf{r},\tau)$ is the interaction potential. The eigenstates of the intrinsic Hamiltonian, $|\eta\rangle$, satisfy the Schrödinger equation [102],

$$\left(e_\eta - H_0\right)|\eta\rangle \quad = 0 \tag{2.55}$$

The orthonormality is,

$$\langle\eta'|\eta\rangle = \int d\tau\, \varphi^*_{\eta'}(\tau)\, \varphi_\eta(\tau) = \delta_{\eta\eta'} \tag{2.56}$$

where $\varphi_\eta\,(\tau)$ $\left(\,\varphi_{\eta'}\,(\tau)\right)^*$ is the wave function corresponding to the state $|\eta\rangle$ ($|\eta\rangle)^*$ in the τ- representation. The interaction potential is split as,

$$U = U' + U'' \tag{2.57}$$

Where U' is diagonal in channel space,

$$U' = \sum_\eta |\eta\rangle\, U'_\eta\, \langle\eta| \tag{2.58}$$

$$U'' = \sum_\eta |\eta\rangle\, U''_{\eta,\eta'}\, \langle\eta'| \tag{2.59}$$

Where

$$U'_\eta(\mathbf{r}) = \int d\tau \left|\varphi_\eta(\tau)\right|^2 U'(\mathbf{r},\tau) \tag{2.60}$$

$$U''_{\eta,\eta'}(\mathbf{r}) = \int d\tau\, \varphi^*_{\eta'}(\tau)\, U''(\mathbf{r},\tau)\, \varphi_{\eta}(\tau) \qquad (2.61)$$

The potential U' is arbitrary, except for the condition of being diagonal in channel space. However, once it is chosen, U'' is given by the relation $U'' = U - U'$. Frequently, it is convenient to choose U' such that U'' is purely off diagonal. In such cases the components of U'' can be written [102],

$$U''_{\eta,\eta'}(\mathbf{r}) = \int d\tau\, \varphi^*_{\eta'}(\tau)\, U''(\mathbf{r},\tau)\, \varphi_{\eta}(\tau) - \delta_{\eta\eta'}\, U'_{\eta}(\mathbf{r}) \qquad (2.62)$$

From the Schrödinger equation, we can start to derive the coupled channel equations,

$$(E - H)\left|\Psi_{\eta}(\eta_0\, \mathbf{k}_0)\right\rangle = 0 \qquad (2.63)$$

and the channel-expansion,

$$\left|\Psi_{\eta}(\eta_0\, \mathbf{k}_0)\right\rangle = \sum_{\eta}\left|\psi_{\eta}(\eta_0\, \mathbf{k}_0)\right\rangle |\eta\rangle \qquad (2.64)$$

The notation $|\Psi(\eta_0\, \mathbf{k}_0)\rangle$ indicates that the collision is started in channel η_0, with wave vector $\mathbf{k}_0$, and the energy scale is chosen such that $e_{\eta_0} = 0$. The Schrödinger equation solution has components $\left|\Psi_{\eta}(\eta_0\, \mathbf{k}_0)\right\rangle$ for both $\eta = \eta_0$ and $\eta \neq \eta_0$, The infinite expansion of Eq. (2.64) is truncated so as to include only the most relevant channels or closed coupling approximation. To account for the loss of flux through neglected channels, One may include an imaginary part in the channel potentials $U'_{\eta}(\mathbf{r})$. To find the wave function, we must write the Hamiltonian as [102].

$$H = H_0 + H' + U'' \qquad (2.65)$$

where

$$H' = T + U' \qquad (2.66)$$

When we put Eqs. (2.64) and (2.65) into Eq. (2.63), and take the scalar product with each intrinsic state $\langle\eta|$, then we get the coupled channel equations,

$$\left(E_\eta - H'_\eta\right)\left|\psi_\eta(\eta_0\,\mathbf{k}_0)\right\rangle = \sum_{\eta'} U''_{\eta,\eta'}(\mathbf{r})\,\left|\psi_{\eta'}(\eta_0\,\mathbf{k}_0)\right\rangle \tag{2.67}$$

or,

$$\left[E_\eta + \frac{\hbar^2}{2\mu}\Delta - U'_\eta(\mathbf{r})\right]\psi_\eta(\mathbf{r}) = \sum_{\eta'} U''_{\eta,\eta'}(\mathbf{r})\,\psi_{\eta'}(\mathbf{r}) \tag{2.68}$$

These equations are usually solved using incoming wave boundary conditions [103].

$$\psi_\eta(\vec{r}) \to T_\eta\, exp\left(-i\int_{r_{abs}}^{r} k'_\eta\left(r'\right)dr'\right), \qquad r \le r_{abs} \tag{2.69}$$

$$\psi_\eta(\vec{r}) \to \frac{i}{2}H_l^{(-)}\left(k_\eta r\right) + \sqrt{\frac{k}{k_\eta}}\,S\,H_l^{(+)}\left(k_\eta r\right), \qquad r > r_{abs} \tag{2.70}$$

Where the potential pocket at $r = r_{abc}$ is minimal, $k_\eta = \sqrt{\frac{2\mu E_\eta}{\hbar^2}}$ and $k = \sqrt{\frac{2\mu E}{\hbar^2}}$ and the local wave number $k'_\eta(r)$ is [104] .

$$k'_\eta(r) = \sqrt{\frac{2\mu}{\hbar^2}\,\left(E_\eta\, - V_{eff}(\mathbf{r}) - U'_\eta(\mathbf{r})\,\right)} \tag{2.71}$$

If we have the transmission coefficients, we can proceed with the rest of the process T_η. The amplitude of scattering $\Re_{tot}(\theta, E)$ is given by [105],

$$\Re_{tot}^{(\eta)}(\theta, E) = \Re_C(\theta, E) + \Re_N^{(\eta)}(\theta, E) \tag{2.72}$$

Were $\Re_C(\theta, E)$ is Coulomb amplitude of scattering, $\Re_N^{(\eta)}(\theta, E)$ nuclear amplitude of scattering. The scattering differential cross section is evaluated as [106] .

$$\frac{d\sigma_{el}}{d\Omega}(\theta, E) = \frac{k_{\eta_0}}{k}\left|\Re_{tot}^{(\eta_0)}(\theta, E)\right|^2 = \frac{k_{\eta_0}}{k}\left|\Re_C(\theta, E) + \Re_N^{(\eta_0)}(\theta, E)\right|^2 \tag{2.73}$$

$$\frac{d\sigma_{in}}{d\Omega}(\theta,E)=\sum_{\eta\neq\eta_0}\frac{k_\eta}{k}\left|\Re_N^{(\eta)}(\theta,E)\right|^2 \tag{2.74}$$

$$\frac{d\sigma_{tot}}{d\Omega}(\theta,E)=\sum_{\eta}\frac{k_\eta}{k}\left|\Re_{tot}^{(\eta)}(\theta,E)\right|^2 \tag{2.75}$$

Rutherford cross section evaluated by [107] .

$$\frac{d\sigma_R}{d\Omega}(\theta,E)=|\Re_C(\theta,E)|^2 \tag{2.76}$$

2.6 Approximate formulation of scattering cross section

We now need to figure out how to define a similar test function for a scattering problem. In the limit of a strong Coulomb field, the cross sections for elastic scattering at $\theta = \pi$ are given by the pure classical approach,

$$\sigma_{el}^{cl}(E,\pi)=\sigma_R(E,\pi)\,\theta(V_b-E) \tag{2.77}$$

where $\sigma_R(E,\pi)$ is known as the Rutherford cross section. The scattering barrier distribution is given by [108].

$$D_{tot}(E)=-\frac{d}{dE}\left(\frac{\sigma_{tot}(E,\pi)}{\sigma_R(E,\pi)}\right) \tag{2.78}$$

In realistic systems, however, the cross section of total scattering deviates from the Rutherford cross section even at energies below the barrier due to the effect of nuclear distortion. Using semi-classical theory [109,110,111], semi-classical formula was derived a for backward scattering that takes the nuclear effect to the leading order into account. The result for a scattering angle θ is as follows:

$$\sigma_{el}(E,\pi)=\sigma_R(E,\pi)\alpha(E,\lambda_C).|S(E,\lambda_C)|^2 \tag{2.79}$$

where $S\ (E,\ \lambda_c)$ denotes the total (Coulomb + nuclear) S-matrix at energy E and angular momentum $\lambda_c = \eta_S cot(\theta/2)$, and is the standard Sommerfeld parameter. It is worth noting that $|S(E, \lambda c)|^2$ is nothing more than the reflection probability of the Coulomb barrier. For $\theta = \pi$, λ_c equals zero, $|S(E, \lambda_c = 0)|^2$ is given by

$$|S(E, \lambda_C\ = 0)|^2 = R(E) = \frac{exp\ \left[-\frac{2\pi}{\hbar\Omega}\ (E - V_b)\right]}{1 + exp\ \left[-\frac{2\pi}{\hbar\Omega}\ (E - V_b)\right]} \qquad (2.80)$$

in terms of the parabolic approximation. $\alpha(E, \lambda c)$ in Eq. (2.81) is given by

$$\alpha(E, \lambda_C\ ) = 1 + \frac{V_N(r_c)}{ka}\frac{\sqrt{2a\pi k\eta_S}}{E}\ \left[1 - \frac{r_c}{Z_P Z_T e^2}\ .2V_N(r_c)\left(\frac{r_c}{a} - 1\right)\right] \qquad (2.81)$$

where $k\ = \sqrt{2\mu E/\hbar^2}\ )$, and μ is the reduce mass of the colliding system .Nuclear potential $V_N(r_c)$ is assessed at the Coulomb's turning point $rc\ = (\eta_S\ + \sqrt{\eta_S^2\ + \lambda_c^2\ })/k$, and a is the nuclear potential's diffuseness parameter.

2.7 Barrier Distribution of Scattering

The extracted distribution of barrier from the excitation function of the measured fusion will provide useful information on the effects of couplings cross-section of fusion comes from the contribution of many channels. The distribution of the barrier of fusion is defined as [112].

$$D_{fus}(E) = \frac{d^2}{dE^2}\ \left[E\ \sigma_{fus}(E)\ \right] \qquad (2.82)$$

To extract the barrier distribution by taking the second derivative of the quantity $E\ \sigma_{fus}(E)$ with respect to E, a very precise measurement of the fusion cross sections is needed. The estimates of absolute scattering at rear angles have related knowledge about the role of chanal couplings in fusion

reactions [113-115]. The sum scattering from the contribution of inelastic and elastic reactions, as well as all other processes from direct reactions including transition and breakup, is known as complete scattering. The probability of transmission through the angular momentum barrier is related to fusion $\ell = 0$, $T_0(E)$, and the large-angle total scattering is related to the probability of reflection, $R_0(E)$. Due to the retention of the reaction flux, $T_0(E) + R_0(E) = 1$, the backscattering of total scattering may be considered to be complementary to the fusion. The total scattering barrier distribution $D_{tot}(E)$ is defined as [115].

$$D_{tot}(E) = -\frac{d}{dE}\left[\frac{\sigma_{tot}}{\sigma_R}(E)\right] \tag{2.83}$$

where σ_{tot}/σ_R is the ratio of total scattering cross sections to Rutherford cross sections. These approaches have the advantage of requiring a numerical assessment of first derivatives rather than second derivatives, as in fusion. In addition, in most cases, the measurement of total and elastic scattering is easier than fusion cross-section.

Chapter Three

Results, Discussion and Conclusions

3.1 Introduction

In this chapter, our calculations of quantum mechanical will be shown involving the scattering reaction of weakly bound nuclei for the systems ^{6}He + ^{120}Sn, ^{6}Li + ^{64}Zn, ^{7}Li + ^{64}Zn, ^{8}B + ^{58}Ni, ^{9}Be + ^{64}Zn, ^{12}C + ^{208}Pb, ^{6}He+^{58}Ni and ^{11}Be+^{197}Au. To investigate the role channel coupling on the calculations of the total and elastic cross section to the Rutherford cross section $\sigma_T, \sigma_{el}/\sigma_R$ was determined with angle center of mass θ_{cm}, and energy center of mass E_{cm}. And the elastic scattering barrier distribution D_{el} was calculated with energy center of mass E_{cm}.

3.2 Results and Discussion

The full quantum mechanical calculations were performed using CC Code. To calculate the total and elastic cross section to the Rutherford cross section $\sigma_T, \sigma_{el}/\sigma_R$, and the elastic scattering barrier distribution D_{el} with energy center of mass E_{cm} numerically using two-point difference method.

The optical nuclear potential was taken to be of Woods-Saxon potential. The Wood-Saxon parameters for Akyüz-Winter potential were taken by least-squares method to experimental data of scattering cross sections by sub-Code for coupled channel calculations, in the present systems, are given in Table (3.1**).**

Table 3.1: Akyüz-Winther potential parameters, high of barrier potential, energy and scattering angle center of mass for some selected systems nuclear reactions.

System	V_0 (MeV)	r_0 (fm)	a_0 (fm)	W_0 (MeV)	r_i (fm)	a_i (fm)	V_b (MeV)	$E_{c.m.}$ (MeV)	$\theta_{c.m.}$ (deg)
^{6}He+^{120}Sn	208.6	1.1	0.64	169.5	1.25	0.56	15.8	16.57	78
^{6}Li+^{64}Zn	51.4	1.2	0.63	110.1	1.25	0.52	12.4	13.5	152
^{7}Li+^{64}Zn	53.7	1.2	0.63	138.9	1.28	0.55	12.1	13.5	144
^{8}B+^{58}Ni	46.6	1.2	0.64	15.5	0.93	0.88	21.5	18.2	122
^{9}Be+^{64}Zn	60.2	1.2	0.62	57.1	0.95	0.65	18.12	16.7	113
^{12}C+^{208}Pb	272.9	1.1	0.63	99.0	0.96	0.35	65	66.1	99
^{6}He+^{58}Ni	48.9	1.2	0.63	99.7	1.27	0.54	10.4	11.05	81
^{11}Be+^{197}Au	88.9	1.2	0.63	50.6	1.1	1.17	32.4	37.1	145

3.2.1 ^{6}He + ^{120}Sn System

In the ^{6}He+^{120}Sn system the elastic cross section to the Rutherford cross section σ_{el}/σ_{R} is determined with angle center of mass θ_{cm} (in Figure 3.1, panel A), energy center of mass E_{cm} (in Figure 3.1, panel B). The elastic scattering barrier distribution D_{el} is calculated with energy center of mass E_{cm} (in Figure 3.1, panel C). The calculations have been performed for the nuclear system ^{6}He+^{120}Sn, where the projectile ^{6}He a halo nucleus containing two neutron on ^{120}Sn target which is a heavy ion, using CDCC method and CC code for all order coupling channels with Akyüz-Winther potential parameters $V_0 = 208.6\,MeV$, $a_0 = 0.64\,fm$, and $r_0 = 1.1\,fm$, $W_0 = 169.5\,MeV$, $a_i = 0.56\,fm$, and $r_i = 1.25\,fm$ which are listed in Table (3.1). The calculations are taken at $E_{cm} =$

$16.57MeV$ with $\theta_{cm} = 78\,deg$ and $V_b = 15.8\,MeV$ [116]. A good agreement for cross section calculations with angle θ_{cm} in coupled state, but the best agreement with data up Coulomb barrier in coupled and no-coupled While down Coulomb barrier, the calculations far from experimental data in two case no coupled and coupled for the cross section and elastic scattering distribution as a function of E_{cm}.

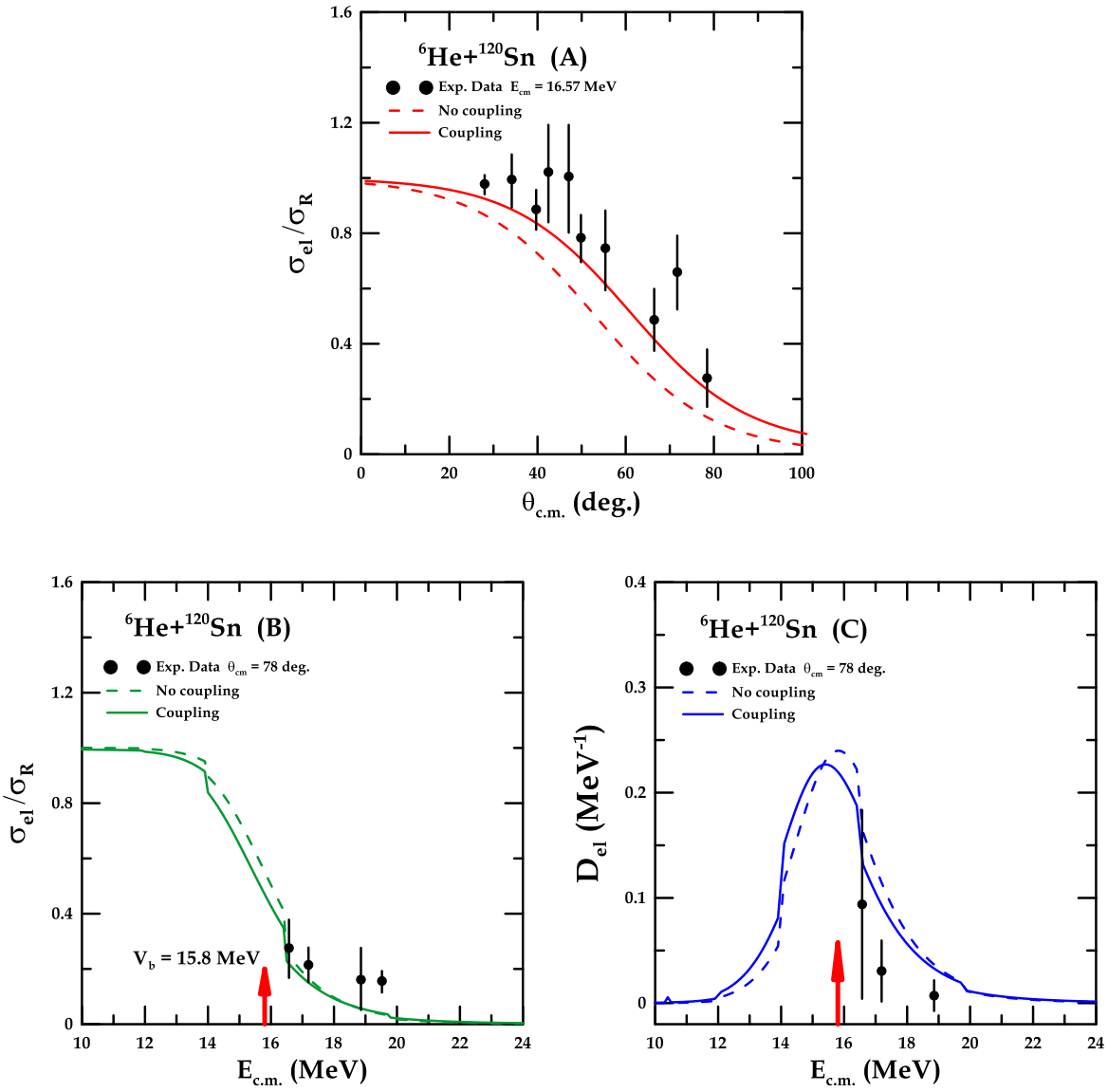

Figure 3.1: Uncoupled channel and coupled channels calculations for ^{6}He+^{120}Sn system by dashed and solid curves respectively : Panel **(A)** The dispersion's elastic differential cross section with the mass angle center, panel **(B)** elastic scattering differential cross section with the energy center of mass, and panel **(C)** elastic scattering barrier distribution with the energy center of mass, the black circles represent experimental data [116].

3.2.2 ^{6}Li + ^{64}Zn System

The calculations have been performed for ^{6}Li+^{64}Zn, where the projectile ^{6}Li consist of three neutrons and three protons, is weakly bound light (stable) nucleus and the target ^{64}Zn medium nucleus. The total scattering cross section to the cross section of Rutherford σ_T/σ_R as a function of the angle center of mass θ_{cm} (in Figure 3.2, panel A), the elastic scattering cross section to Rutherford cross section σ_{el}/σ_R and the elastic scattering barrier distribution D_{el} as a function of energy center of mass E_{cm} (in Figure 3.2, panels B and C). The best fitting parameters for Akyüz-Winther potential are $V_0 = 51.4$ MeV, $a_0 = 0.63$ fm, $r_0 = 1.2$ fm, $W_0 = 110.1$ MeV, $a_i = 0.52$ fm, $r_i = 1.25$ fm, and height barrier $V_b = 12.4$ MeV, which are listed in Table (3.1). The comparison between theoretical results and the measured data in perfect match under Coulomb barrier of coupled channels case and above barrier in no-coupled case for the elastic scattering cross section to Rutherford cross section σ_{el}/σ_R and the elastic scattering barrier distribution D_{el} as a function of energy center of mass E_{cm}. Excellent agreement for the total scattering cross section to the cross section of Rutherford σ_T/σ_R as a function of the angle center of mass θ_{cm} with no coupled and coupled channel until the values reach the angle limit at $\theta_{cm} = 110\ deg$, are deviate slightly from data and closer of no-coupled state.

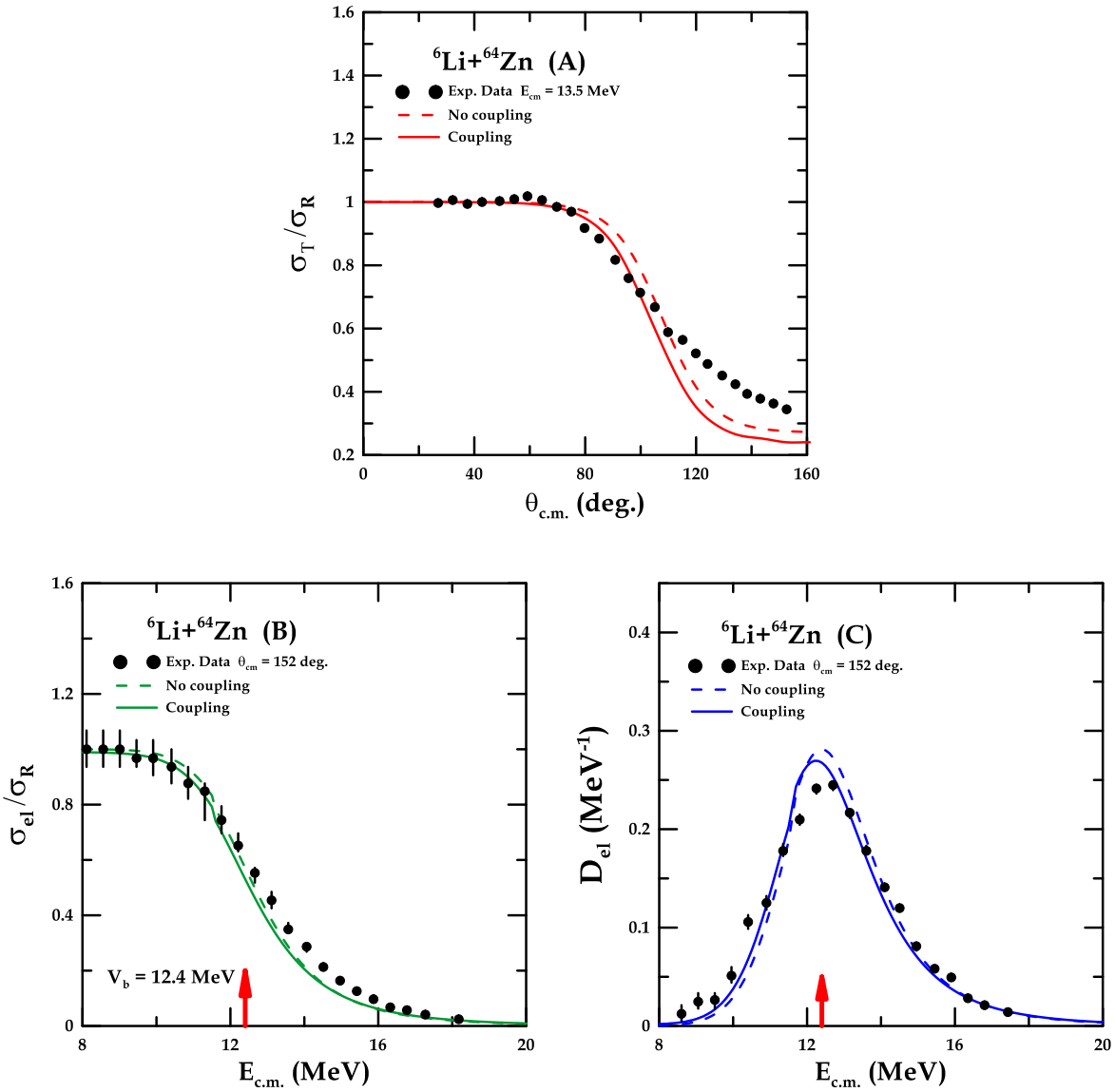

Figure 3.2: Uncoupled channel and coupled channels calculations for ^{6}Li+^{90}Zr system by dashed and solid curves respectively: Panel **(A)** total scattering differential cross section with the mass angle center, panel (B) elastic scattering differential cross section with energy center of mass, and panel **(C)** elastic scattering barrier distribution with the energy center of mass, the black circles represent experimental data [117].

3.2.3 ^{7}Li + ^{64}Zn System

In figure 3.3, the total cross section to the Rutherford cross section (σ_T/σ_R) is determined with angle center of mass θ_{cm} in (panel A) and the elastic scattering cross section to the Rutherford cross section (σ_{el}/σ_R) with energy center of mass E_{cm} in (panel B). The elastic scattering barrier distribution D_{el} as a function of energy center of mass E_{cm} in (panel C). The calculations have been performed by using CC code for all order coupling channels for the nuclear system ^{7}Li+^{64}Zn. The projectile ^{7}Li is made up of four neutrons and three protons is weakly bound light (stable) nucleus and the target ^{64}Zn, with Akyüz-Winther potential parameters $V_0 = 53.7\ MeV$, $a_0 = 0.63\ fm$, $r_0 = 1.2\ fm$, $W_0 = 138.9\ MeV$, $a_i = 0.55\ fm$, $r_i = 1.28\ fm$ and $V_b = 12.1\ MeV$, which are listed in Table (3.1). In the case of coupled channels, the excellent match between theoretical calculations and experimental data with slight deviation after angle 85 for the total cross section to the Rutherford cross section with angle center of mass θ_{cm}. All calculations of the elastic scattering cross section to the Rutherford cross section and elastic scattering barrier distribution D_{el} in excellent agreement for coupling and no-coupling cases above and under Coulomb barrier.

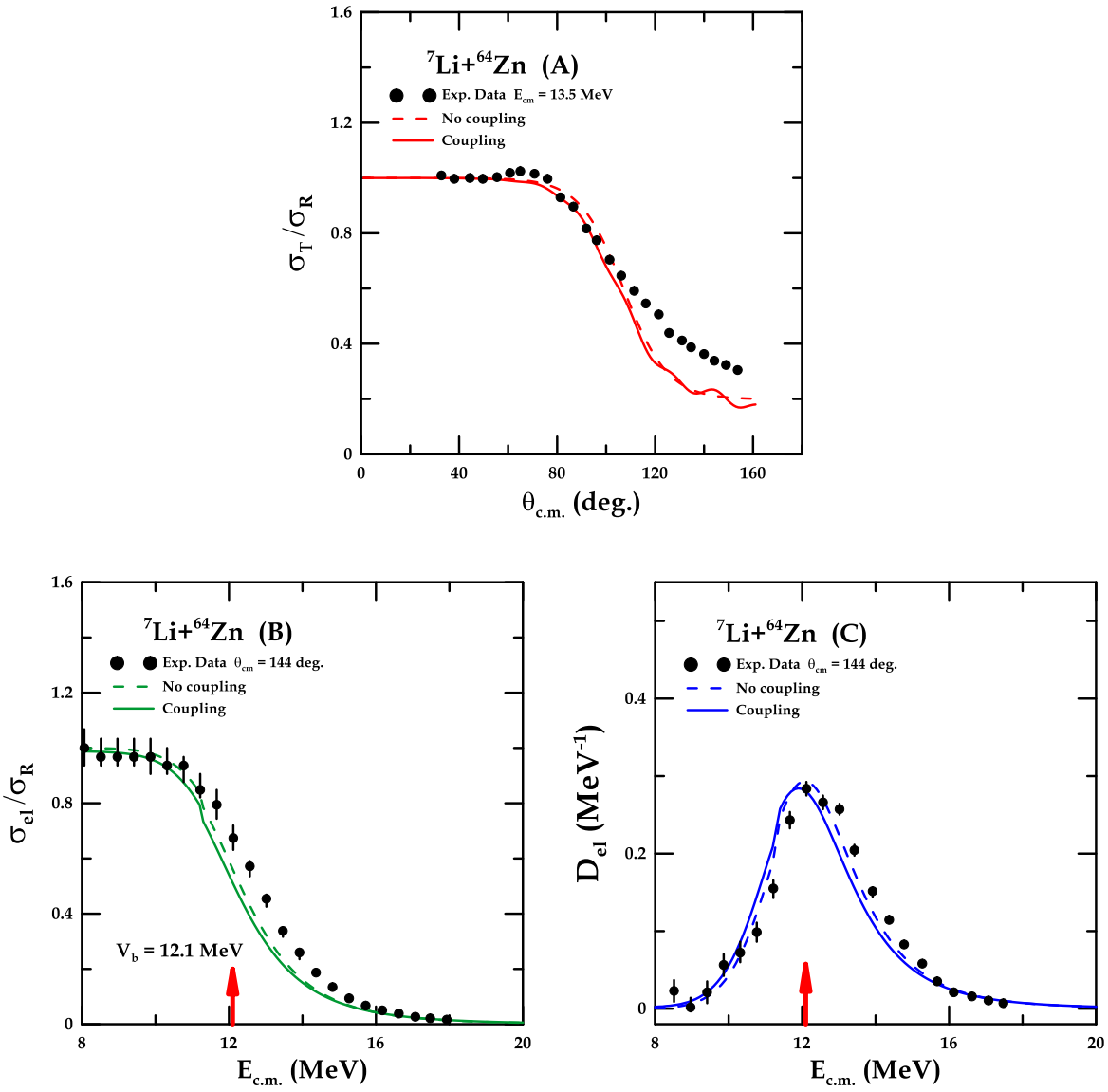

Figure 3.3 : Uncoupled channel and coupled channels calculations for ^{7}Li+^{64}Zn system by dashed and solid curves respectively : Panel **(A)** total differential cross section of the dispersion with the mass angle center, panel **(B)** elastic scattering differential cross section with the energy center of mass, and panel **(C)** elastic scattering barrier distribution with the energy center of mass, the black circles represent experimental data [118].

3.2.4 ^{8}B + ^{58}Ni System

The cross section of scattering as a function of angle center of mass θ_{cm} and as a function of energy center of mass $E_{cm}$to the cross section of Rutherford σ_{el}/σ_R is shown (in Figure 3.4, panel A and B) for the ^{8}B+^{58}Ni system. The elastic scattering barrier distribution D_{el} is calculated with energy center of mass E_{cm} (in Figure 3.4, panel C). The Akyüz-Winther potential parameters are taken; $V_0 = 46.6$ MeV, $a_0 = 0.64$ fm, and $r_0 = 1.2$ fm, $W_0 = 15.5$ MeV, $a_i = 0.88$ fm, $r_i = 0.93$ fm, and $V_b = 21.5$ MeV from [119], which are listed in Table (3.1). The projectile ^{8}B weakly bound halo (unstable) nucleus on the target ^{58}Ni .The calculations in panel A, B and C, for all order coupling channels in perfect agreement with experimental data. But get in bag splay in cross section of scattering to the cross section of Rutherford σ_{el}/σ_R as a function of angle center of mass θ_{cm} over angle 122° and as a function of energy center of mass E_{cm} at sub-barrier region in no-coupling state. As well as elastic scattering barrier distribution D_{el} calculations with energy center of mass E_{cm} in single channel case no match with experimental data.

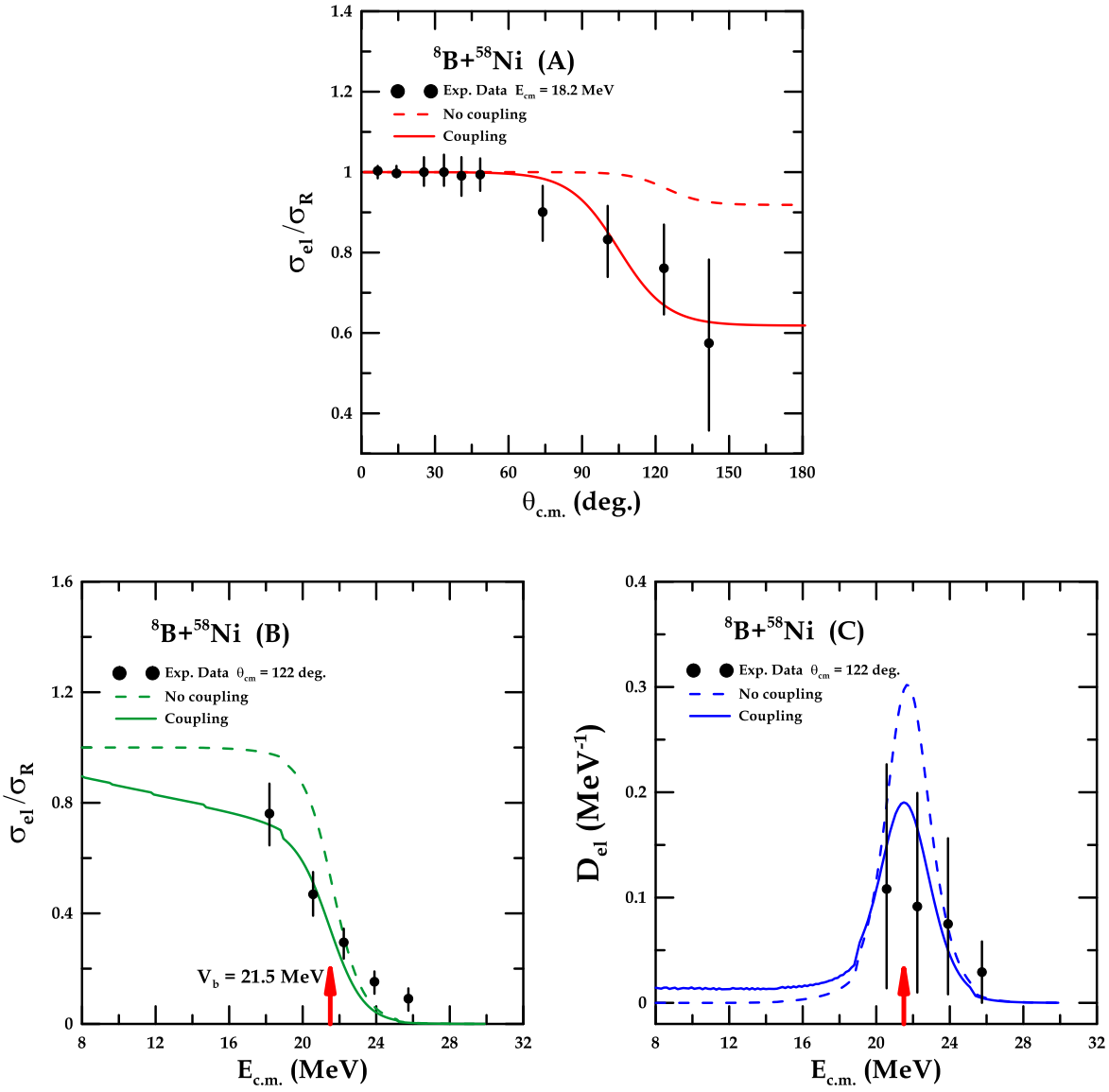

Figure 3.4: Uncoupled channel and coupled channels calculations for $^{8}B+^{58}Ni$ system by dashed and solid curves respectively: Panel **(A)** elastic scattering differential cross section with the mass angle center, panel **(B)** elastic differential energy center of mass cross section scattering, and panel **(C)** elastic scattering barrier distribution with the energy center of mass, the black circles represent experimental data [119].

3.2.5 ^{9}Be + ^{64}Zn System

In ^{9}Be+^{64}Zn system, the elastic cross sections vary as a function of the angle center of mass to the Rutherford differential cross section (σ_{el}/σ_{R}) is determined with angle center of mass θ_{cm} (in Figure 3.5, panel A), energy center of mass E_{cm} (in Figure 3.5, panel B). The elastic scattering barrier distribution D_{el} is calculated with energy center of mass E_{cm} (in Figure 3.5, panel C). The calculations have been performed for the nuclear system ^{9}Be+^{64}Zn, where the projectile ^{9}Be is weakly bound light (stable) nucleus and the target ^{64}Zn, using CDCC method and CC code for all order coupling channels with Akyüz-Winther potential parameters $V_0 = 60.2MeV$, $a_0 = 0.62fm$, and $r_0 = 1.2\,fm$, $W_0 = 57.1\,MeV$, $a_i = 0.65\,fm$, and $r_i = 0.95\,fm$, and $V_b = 18.12\,MeV$ [120], which are listed in Table (3.1). At $E_{cm} = 16.7MeV$, the elastic cross sections to the Rutherford differential cross section with angle center of mass θ_{cm} in excellent match with experimental data in uncoupled and coupled channels. Acceptable match between theoretical calculations and experimental data for the calculations of the elastic cross sections to the Rutherford differential cross section with energy center of mass E_{cm} and the elastic scattering barrier distribution D_{el} in coupled state which that best from single state.

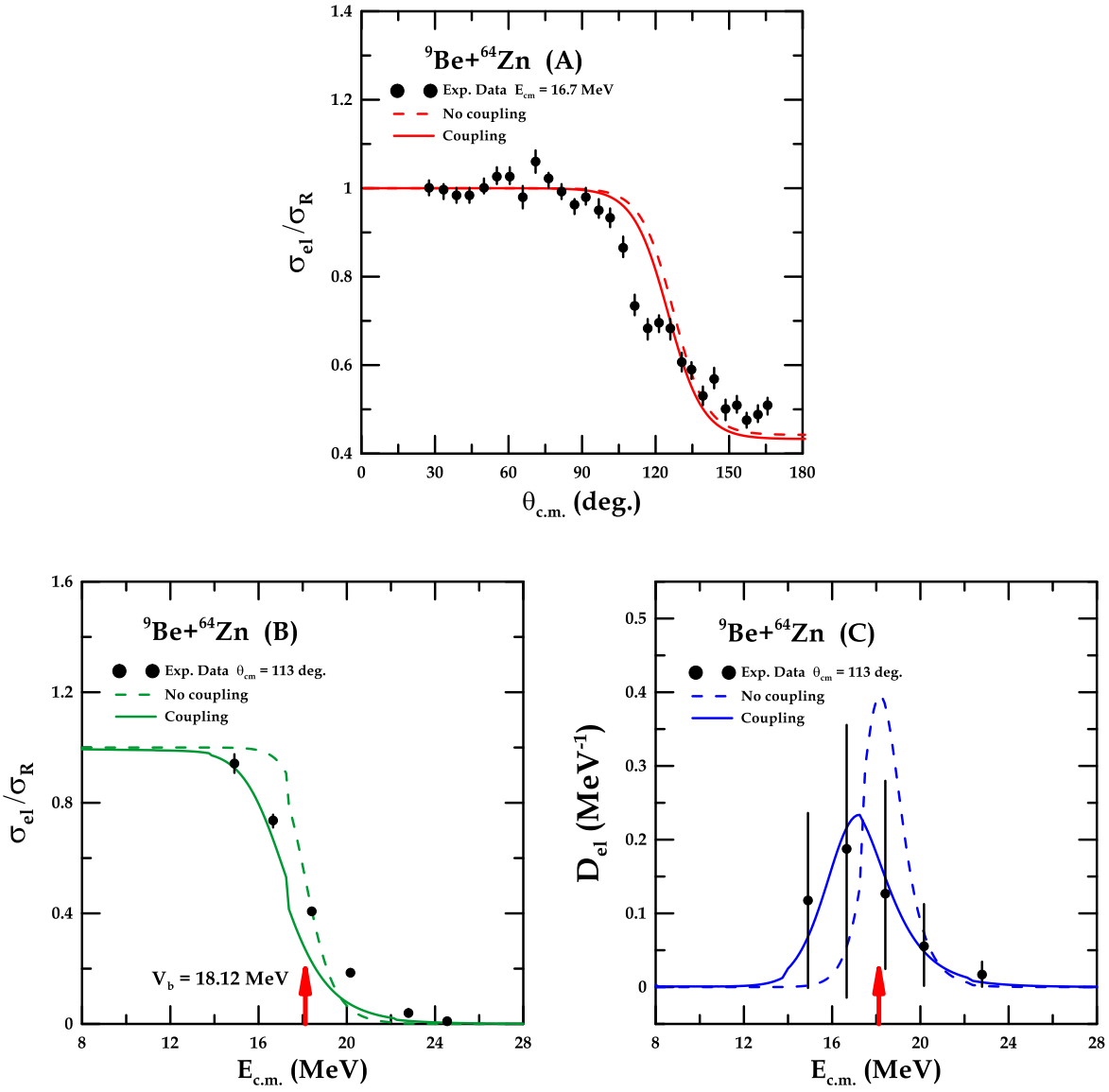

Figure 3.5: Uncoupled channel and coupled channels calculations for ^{9}Be+^{64}Zn system by dashed and solid curves respectively: Panel **(A)** elastic scattering differential cross section with the mass angle center, panel **(B)** differential cross section of elastic scattering with energy center of mass, and panel **(C)** elastic scattering barrier distribution with the energy center of mass, the black circles represent experimental data [120].

3.2.6 $^{12}C + ^{208}Pb$ System

Figure 3.6, the elastic scattering cross sections to the Rutherford cross section (σ_{el}/σ_R) as a function of angle center of mass θ_{cm} (in panel A), and with energy center of mass E_{cm} (in panel B). The elastic scattering barrier distribution D_{el} was calculated with energy center of mass E_{cm} (in panel C). The calculations have been performed for the nuclear system $^{12}C + ^{208}Pb$ where the projectile ^{12}C is weakly bound light (stable) nucleus and the target ^{208}Pb is heavy ion. The best fitting of Akyüz-Winther potential parameters are $V_0 = 272.9 MeV$, $a_0 = 0.63 fm$, $r_0 = 1.1\ fm$, $W_0 = 99.0\ MeV$, $a_i = 0.35\ fm$, and $r_i = 0.96\ fm$ and $V_b = 65\ MeV$ [121], which are listed in Table (3.1). In the case of coupled channels, the excellent match between theoretical calculations and experimental data was for all calculations of this method.

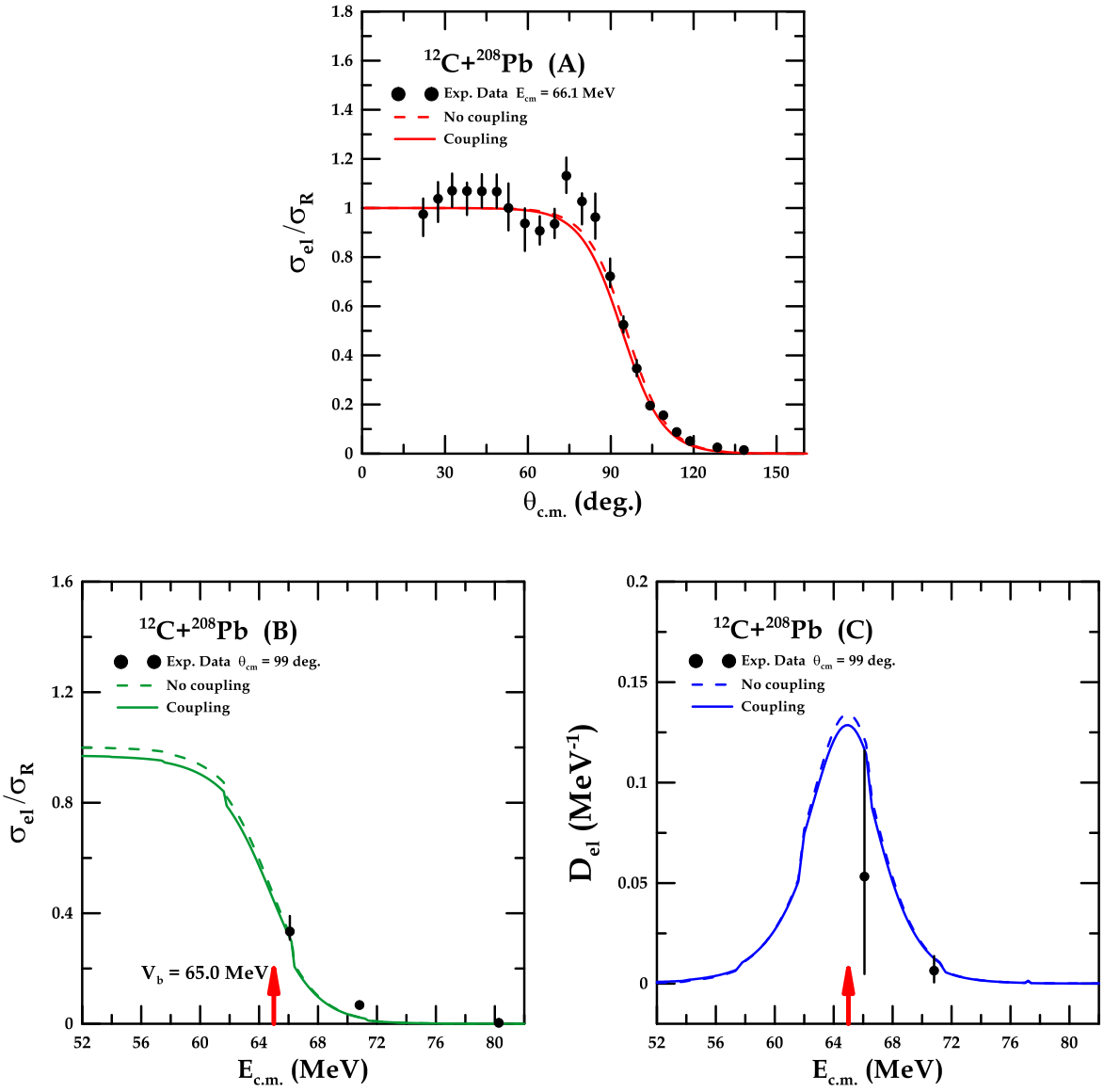

Figure 3.6: Uncoupled channel and coupled channels calculations for ^{12}C + ^{208}Pb system by dashed and solid curves respectively: Panel **(A)** elastic scattering differential cross section with the mass angle center, panel **(B)** differential cross section of elastic scattering with energy center of mass, and panel **(C)** elastic scattering barrier distribution with the energy center of mass, the black circles represent experimental data [121].

3.2.7 ^{6}He + ^{58}Ni System

Figure 3.7 (A) shows the cross section of scattering as a function of angle center of mass to the cross section of Rutherford σ_{el}/σ_R with angle center of mass θ_{cm} for the ^{6}He + ^{58}Ni system, the cross section of elastic scattering to the cross section of Rutherford σ_{el}/σ_R is calculated with energy center of mass E_{cm} (in Figure 3.7, panel B). The elastic scattering barrier distribution D_{el} was calculated with energy center of mass E_{cm} (in Figure 3.7, panel C). The results have been done for ^{6}He + ^{58}Ni reaction, where the projectile ^{6}He is weakly bound (unstable) nucleus consisting of two neutron halo nucleus and the target ^{58}Ni is taken. using CDCC method and CC code for all order coupling channels with Akyüz-Winther potential parameters $V_0 = 48.9$ MeV, $a_0 = 0.63$ fm, $r_0 = 1.2$ fm, $W_0 = 99.7$ MeV, $a_i = 0.54$ fm, and $r_i = 1.27$ fm, and $V_b = 10.4$ MeV [122] which are listed in Table (3. 1). The best fitting between theoretical predictions and the measured data is obtained for this system at $\theta_{cm} = 81\ deg\ and\ E_{cm} = 11.05\ MeV$ in a good agreement of single and coupled channels for calculations in the cross section of scattering as a function of angle center of mass to the cross section of Rutherford σ_{el}/σ_R with angle center of mass θ_{cm}. The elastic scattering of cross sections and barrier distribution D_{el} with energy center of mass E_{cm} in coupled channel are the best.

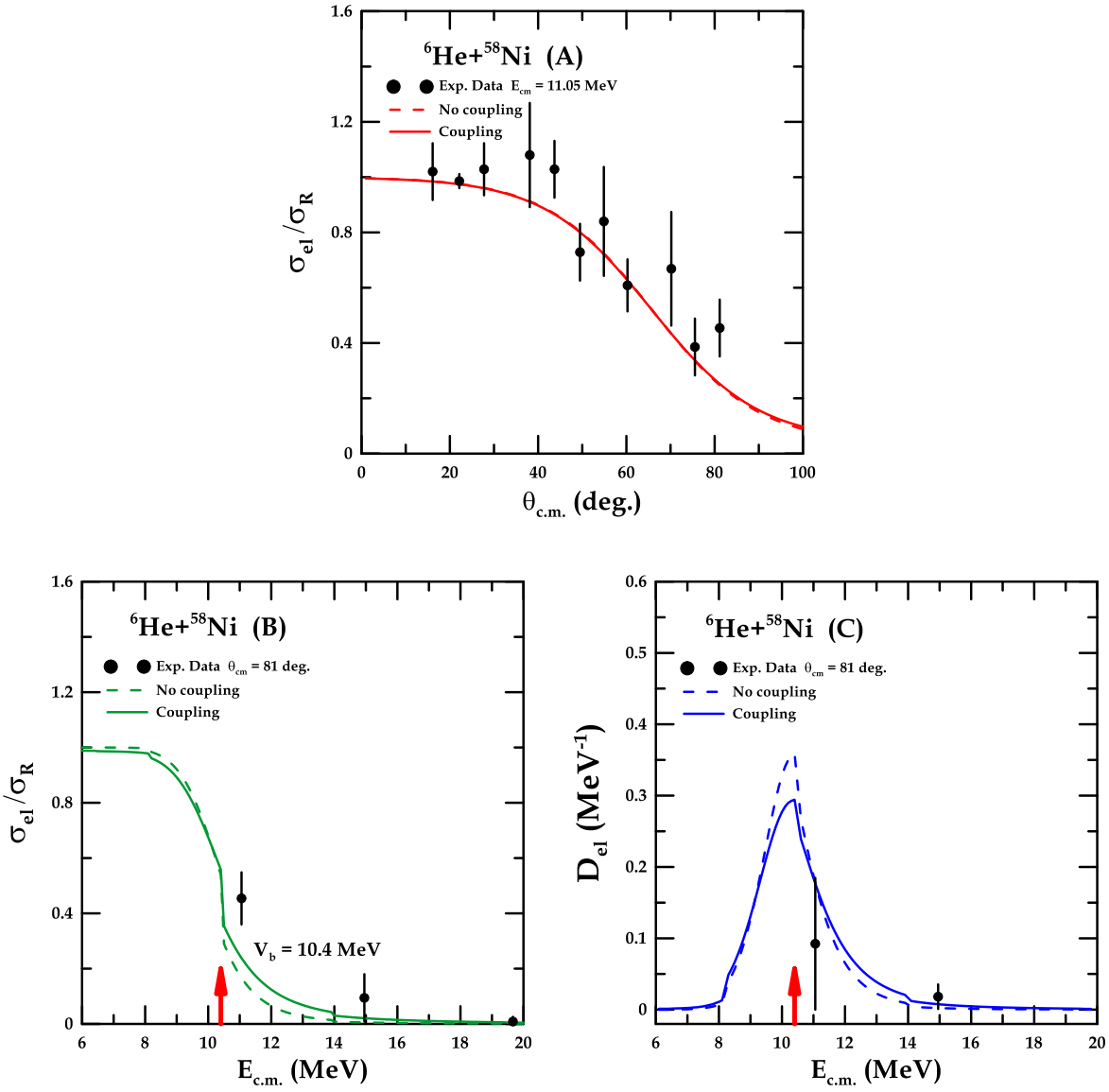

Figure 3.7: Uncoupled channel and coupled channels calculations for ^{6}He + ^{58}Ni system by dashed and solid curves respectively: Panel **(A)** elastic scattering cross section with the mass angle center, panel **(B)** cross section of elastic scattering with energy center of mass, and panel **(C)** elastic scattering barrier distribution with the energy center of mass, the black circles represent experimental data [122].

3.2.8 ^{11}Be + ^{197}Au System

In the ^{11}Be + ^{197}Au system, the results of this reaction are taken of the elastic cross section to the Rutherford cross section σ_T / σ_R is determined with angle center of mass θ_{cm} (in Figure 3.8, panel A), energy center of mass E_{cm} (in Figure 3.8, panel B). The elastic scattering barrier distribution D_{el} is calculated with energy center of mass E_{cm} (in Figure 3.8, panel C). The calculations have been performed for the nuclear system ^{11}Be + ^{197}Au, where the projectile ^{11}Be is one neutron halo (unstable) nucleus and the target ^{197}Au is heavy ion, with Akyüz-Winther potential parameters $V_0 = 88.9\ MeV$, $a_0 = 0.63\ fm$, $r_0 = 1.2\ fm$, $W_0 = 50.6\ MeV$, $a_0 = 1.17\ fm$, $r_0 = 1.1\ fm$ and $V_b = 32.4\ MeV$, which are listed in Table (3.1). Acceptable agreement between theoretical calculations and experimental data below the Coulomb barrier in coupled and uncoupled calculations with found variation for the total elastic cross section to the Rutherford cross section with angle center of mass θ_{cm} at coupled state.

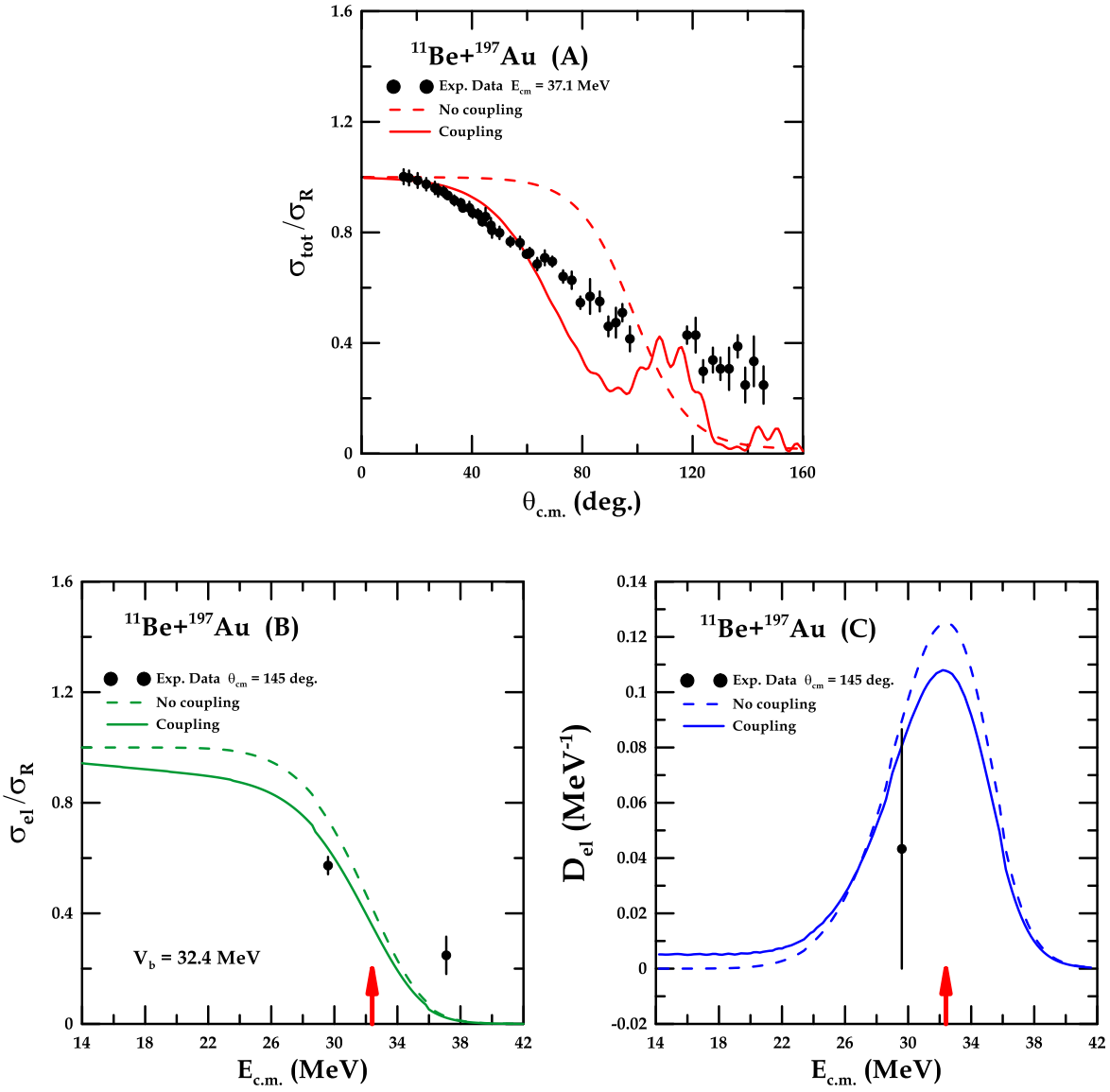

Figure 3.8: Uncoupled channel and coupled channels calculations for ^{11}Be + ^{197}Au system by dashed and solid curves respectively: Panel (A) total scattering cross section with the mass angle center, panel (B) cross section of elastic scattering with energy center of mass, and panel (C) elastic scattering barrier distribution with the energy center of mass, the black circles represent experimental data [123].

3.3 Conclusions

1. The effect of channels coupling with breakup channel on the ratio of total scattering cross section to Rutherford cross section σ_{tot}/σ_R and the distribution of the Coulomb barrier D_{el} (MeV^{-1}) calculations were given a good match with the experimental data.
2. In the system, ^{7}Li + ^{64}Zn, the best and suitable agreement of channels coupling with breakup channel has been found fit to experimental values better than the other results of CDCC analysis.
3. At incident energies near the Coulomb barrier, the elastic scattering of the two neutron halo nucleus ^{6}He on heavy targets deviates significantly in no-coupled state from coupled state.
4. we conclude that the breakup effect is very important for weakly bound projectiles, suppressed on medium and heavy target nuclei above the Coulomb barrier, and, oppositely, is enhanced for some weakly bound projectiles at energies near and below the Coulomb barrier.
5. In ^{6}Li + ^{64}Zn System, the comparison between theoretical results and the measured data has a perfect matching under Coulomb barrier of coupled channels case and above barrier in no-coupled case for all calculation of this system.
6. In ^{12}C + ^{208}Pb system, the elastic scattering of the projectile (stable) nucleus on heavy target is enhanced at energies above the Coulomb barrier.
7. In ^{11}Be + ^{197}Au system, the total and elastic scattering of the projectile (one neutron halo) nucleus on heavy target is suppression at energies below the Coulomb barrier.

3.4 Future works

1. Using elastic scattering with the double folding model (DFM) and dynamic polarization effective potential to perform the study and compare it with the present calculations.
2. Develop CC code to calculate cross-sections and distributions for heavy and medium systems.
3. Using semiclassical approximation in scattering cross-sections and distribution calculations and its comparison with quantum mechanics calculations.

References

References

[1] Bertulani, C. A., and Danielewicz, P. (2019). *Introduction to nuclear reactions*. CRC Press.

[2] Gomes, P. R. S., Lubian, J., Canto, L. F., Otomar, D. R., Junior, D. M., de Faria, P. N., and Hussein, M. S. (2016). Reactions with weakly bound nuclei, at near barrier energies, and the breakup and transfer influences on the fusion and elastic scattering. *few-body Systems*, *57*(3), 165-176.

[3] Siemens, P. J. (1983). Liquid–gas phase transition in nuclear matter. *Nature*, *305*(5933), 410-412.

[4] Bertulani, C. A. (2009). Nuclear reactions. *arXiv preprint arXiv:0908.3275*.

[5] Gomes, P. R. S., Junior, D. M., Canto, L. F., Lubian, J., and De Faria, P. N. (2016). Reduction Methods for Total Reaction Cross Sections. *Few-Body Systems*, *57*(3), 205-216.

[6] Vaz, L. C., Alexander, J. M., and Satchler, G. R. (1981). Fusion barriers, empirical and theoretical: Evidence for dynamic deformation in subbarrier fusion. *Physics reports*, *69*(5), 373-399.

[7] Pollarolo, G., and Winther, A. (2000). Fusion excitation functions and barrier distributions: A semiclassical approach. *Physical Review C*, *62*(5), 054611.

[8] Beckerman, M. (1985). Subbarrier fusion of atomic nuclei. *Physics Reports*, *129*(3), 145-223.

[9] Esbensen, H. (1981). Fusion and zero-point motions. *Nuclear Physics A*, *352*(1), 147-156.

[10] Arnikar, H. J. (1995). *Essentials of nuclear chemistry* (No. 1653). New Age International.

[11] Patel, S. B. (1991). *Nuclear physics: an introduction*. New Age International.

[12] Blatt, J. M and Weisskopf, V. F. (1979) *Theoretical Nuclear Physics* (Dover Publications)

[13] Ryan, S. G., and Norton, A. J. (2010). *Stellar evolution and nucleosynthesis*. Cambridge University Press.

[14] Fröbrich, P., and Lipperheide, R. (1996). *Theory of nuclear reactions* (Vol. 18). Courier Corporation.

[15] Shultis , J.K. and Faw ,R. E. (2016). Fundamentals of Nuclear Science and Engineering Third Edition, CRC press.

[16] Nagarajan, M. A., Mahaux, C. C., and Satchler, G. R. (1985). Dispersion relation and the low-energy behavior of the heavy-ion optical potential. *Physical review letters*, *54*(11), 1136.

[17] Brandan, M. E., and Satchler, G. R. (1997). The interaction between light heavy-ions and what it tells us. *Physics reports*, *285*(4-5), 143-243.

[18] Mahaux, C., Ngo, H., and Satchler, G. R. (1986). Causality and the threshold anomaly of the nucleus-nucleus potential. *Nuclear Physics A*, *449*(2), 354-394.

[19] Lubian, J., Correa, T., Aguilera, E. F., Canto, L. F., Gomez-Camacho, A., Quiroz, E. M., and Gomes, P. R. S. (2009). Effects of breakup couplings on ^{8}B + ^{58}Ni elastic scattering. *Physical Review C*, *79*(6), 064605.

[20] Santra, S., Kailas, S., Ramachandran, K., Parkar, V. V., Jha, V., Roy, B. J., and Shukla, P. (2011). Reaction mechanisms involving weakly bound ^{6}Li and ^{209}Bi at energies near the Coulomb barrier. *Physical Review C*, *83*(3), 034616.

[21] Gomes, P. R. S., Padron, I., Niello, J. F., Martí, G. V., Rodríguez, M. D., Capurro, O. A., and Hussein, M. S. (2005). Fusion, break-

up and elastic scattering of weakly bound nuclei. *Journal of Physics G: Nuclear and Particle Physics*, *31*(10), S1669.

[22] Hussein, M. S., Gomes, P. R. S., Lubian, J., and Chamon, L. C. (2006). New manifestation of the dispersion relation: Breakup threshold anomaly. *Physical Review C*, *73*(4), 044610.

[23] Maciel, A. M. M., Gomes, P. R. S., Lubian, J., Anjos, R. M., Cabezas, R., Santos, G. M., and Tenreiro, C. (1999). Influence of the 6, 7 Li breakup process on the near barrier elastic scattering by heavy nuclei. *Physical Review C*, *59*(4), 2103.

[24] Lubian, J., Padrón, I., Gomes, P. R. S., Maciel, A. M. M., Anjos, R. M., Moraes, S. B., and Added, N. (2001). Low-lying inelastic channel couplings versus breakup effects on the fusion cross section. *Physical Review C*, *64*(2), 027601.

[25] Figueira, J. M., Niello, J. F., Arazi, A., Capurro, O. A., Carnelli, P., Fimiani, L., and Gomes, P. R. S. (2010). Energy dependence of the optical potential of weakly and tightly bound nuclei as projectiles on a medium-mass target. *Physical Review C*, *81*(2), 024613.

[26] Nigussie, B. (2012). *Complete and incomplete fusion studies in some $^{14}N+\ ^{59}Co$ systems* (Doctoral dissertation, Addis Ababa University).

[27] Stock, R. (2009). Encyclopedia of applied high energy and particle physics.

[28] Desalegn, K. (2013). *Complete and Incomplete Fusion Reactions in $^{16}O+\ ^{93}Nb$ Systems at Various Projectile Energies* (Doctoral dissertation, Addis Ababa University).

[29] Savard, G., Davids ,C.N. and Lister, C. J. (2004).Proceedings of the Sixth International Conference on Radioactive Nuclear Beams, Nuclear Physics A 746, 522

[30] B. Nigussie ,COMPLETE AND INCOMPLETE FUSION STUDIES IN SOME ^{14} N + ^{59} Co SYSTEMS, M.Sc. Thesis, Addis Ababa University, (2012).

[31] Hansen, P. G., and Sherrill, B. M. (2001). Reactions and single-particle structure of nuclei near the drip lines. *Nuclear Physics A*, *693*(1-2), 133-168.

[32] Kanungo,R. The Magic of Star Dust - Exploring Exotic Nuclei, TRIUMF Financial Report 2007–2008, p. 10.

[33] Steppenbeck, D., Deacon, A. N., Freeman, S. J., Janssens, R. V. F., Zhu, S., Carpenter, M. P., and Varley, B. J. (2010). High-spin structures in the neutron-rich isotopes Mn 57− 60. *Physical Review C*, *81*(1), 014305.

[34] Deacon, A. N., Steppenbeck, D., Zhu, S., Freeman, S. J., Janssens, R. V. F., Carpenter, M. P., and Yang, Y. C. (2011). Single-particle and collective structures in Cr 55 and V 55. *Physical Review C*, *83*(6), 064305.

[35] Riisager, K., Fedorov, D. V., and Jensen, A. S. (2000). Quantum halos. *EPL (Europhysics Letters)*, *49*(5), 547.

[36] Moon, C. B. (2014). A nuclear physics program at the Rare Isotope Beams Accelerator Facility in Korea. *AIP Advances*, *4*(4), 041001.

[37] Thibault, C., Klapisch, R., Rigaud, C., Poskanzer, A. M., Prieels, R., Lessard, L., and Reisdorf, W. (1975). Direct measurement of the masses of Li 11 and Na 2 6− 3 2 with an on-line mass spectrometer. *Physical Review C*, *12*(2), 644.

[38] Wouters, J. M., Kraus, R. H., Vieira, D. J., Butler, G. W., and Löbner, K. E. G. (1988). Direct mass measurements of the neutron-rich light isotopes of lithium through fluorine. *Zeitschrift für Physik A Atomic Nuclei*, *331*(3), 229-233.

[39] Smith, M., Brodeur, M., Brunner, T., Ettenauer, S., Lapierre, A., Ringle, R., and Dilling, J. (2008). First Penning-trap mass measurement of the exotic halo nucleus ^{11}Li. *Physical review letters*, *101*(20), 202501.

[40] Hansen, P. G., and Jonson, B. (1987). The neutron halo of extremely neutron-rich nuclei. *EPL (Europhysics Letters)*, *4*(4), 409.

[41] Bertulani, C. A., Canto, L. F., and Hussein, M. S. (1993). The structure and reactions of neutron-rich nuclei. *Physics Reports*, *226*(6), 281-376.

[42] Hansen, P. G. (1995). AS Jensen ad B. Jonson. *Ann. Rev. Nucl. Part. Sci*, *45*, 591.

[43] Fedorov, D. V., Jensen, A. S., and Riisager, K. (1994). Efimov states in halo nuclei. *Physical review letters*, *73*(21), 2817.

[44] Al-Khalili, J. S., and Roeckl, E. (Eds.). (2004). *The Euroschool Lectures on Physics with Exotic Beams* (Vol. 1). Springer Science & Business Media.

[45] Audi, G., and Wapstra, A. H. (1995). The 1995 update to the atomic mass evaluation. *Nuclear Physics A*, *595*(4), 409-480.

[46] Tanihata, I. (1996). Neutron halo nuclei. *Journal of Physics G: Nuclear and Particle Physics*, *22*(2), 157.

[47] Minamisono, T., Ohtsubo, T., Minami, I., Fukuda, S., Kitagawa, A., Fukuda, M., and Kitagawa, H. (1992). Proton halo of ^{8}B disclosed by its giant quadrupole moment. *Physical review letters*, *69*(14), 2058.

[48] Baye, D., Descouvemont, P., and Timofeyuk, N. K. (1994). Matter densities of 8B and 8Li in a microscopic cluster model and the proton-halo problem of 8B. *Nuclear Physics A*, *577*(3-4), 624-640.

[49] Ozawa, A., Kobayashi, T., Sato, H., Hirata, D., Tanihata, I., Yamakawa, O., and Wieman, H. (1994). Interaction cross sections and radii of the mass number A= 17 isobar (^{17}N, ^{17}F, and ^{17}Ne). *Physics Letters B*, *334*(1-2), 18-22.

[50] Karataglidis, S., and Bennhold, C. (1998). Probing proton halos through pion photoproduction. *Physical review letters*, *80*(8), 1614.

[51] Gomes, P. R. S., Padron, I., Rodriguez, M. D., Marti, G. V., Anjos, R. M., Lubian, J., and Hussein, M. S. (2004). Fusion, reaction and break-up cross sections of weakly bound projectiles on 64Zn. *Physics Letters B*, *601*(1-2), 20-26.

[52] Gomes, P. R. S., Rodriguez, M. D., Martí, G. V., Padron, I., Chamon, L. C., Niello, J. F., and Hussein, M. S. (2005). Effect of the breakup on the fusion and elastic scattering of weakly bound projectiles on ^{64}Zn. *Physical Review C*, *71*(3), 034608.

[53] Beck, C., Keeley, N., and Diaz-Torres, A. (2007). Coupled-channel effects in elastic scattering and near-barrier fusion induced by weakly bound nuclei and exotic halo nuclei. *Physical Review C*, *75*(5), 054605.

[54] Canham, D. L., and Hammer, H. W. (2008). Universal properties and structure of halo nuclei. *The European Physical Journal A*, *37*(3), 367-380.

[55] Kucuk, Y., Boztosun, I., and Keeley, N. (2009). Onset of nuclear structure effects in near-barrier elastic scattering of weakly bound nuclei: ^{6}He and ^{6}Li compared. *Physical Review C*, *79*(6), 067601.

[56] Beck, C., Rowley, N., Papka, P., Courtin, S., Rousseau, M., Souza, F. D. A., and Hagino, K. (2010). Reaction mechanisms for weakly-bound, stable nuclei and unstable, halo nuclei on medium-mass targets. *Nuclear Physics A*, *834*(1-4), 440c-445c.

[57] A.T. Rudchik, Yu.O. Shyrma, K.W. Kemper, K. Rusek, E.I. Koshchy, S. Kliczewski, B.G. Novatsky, O.A. Ponkratenko, E. Piasecki, G.P. Romanyshyna, Yu.M. Stepanenko, I. Strojek, S.B. Sakuta,A. Budzanowski, L. G_lowacka, I. Skwirczy´nska, R. Siudak, J. Choi´nski, and A. Szczurek, Isotopic effects in elastic and inelastic $^{12}C + ^{16,18}O$ scattering, Eur. Phys. J. A 44, 221–231 (2010).

[58] Barioni, A., Zamora, J. C., Guimaraes, V., Paes, B., Lubian, J., Aguilera, E. F., and Jiang, H. (2011). Elastic scattering and total reaction cross sections for the ^{8}B, ^{7}Be , and $^{6}Li + ^{12}C$ systems. *Physical Review C*, *84*(1), 014603.

[59] Cubero, M., Fernández-García, J. P., Rodríguez-Gallardo, M., Acosta, L., Alcorta, M., Alvarez, M. A. G., and Walden, P. (2012). Do Halo Nuclei Follow Rutherford Elastic Scattering at Energies Below the Barrier? The Case of ^{11}Li. *Physical review letters*, *109*(26), 262701.

[60] Woodard, A. E., Figueira, J. M., Otomar, D. R., Niello, J. F., Lubian, J., Arazi, A., and Gomes, P. R. S. (2012). Breakup coupling effects on near-barrier inelastic scattering of the weakly bound 6Li projectile on a 144Sm target. *Nuclear Physics A*, *873*, 17-27.

[61] Otomar, D. R., Gomes, P. R. S., Lubian, J., Canto, L. F., and Hussein, M. S. (2013). Nuclear and Coulomb breakup of the weakly bound 6 Li nucleus with targets in the range from A= 59 to 208. *Physical Review C*, *87*(1), 014615.

[62] Yang, X. P., Zhang, G. L., and Zhang, H. Q. (2013). Systematic study of reaction functions of weakly bound nuclei. *Physical Review C*, *87*(1), 014603.

[63] N. N. Deshmukh, V. Guimar˜aes, E. Crema, D. Abriola, A. Arazi, E. de Barbar´a, O. A. Capurro, M. A. Cardona, J. Gallardo, D. Hojman, G. V. Mart´ı, A. J. Pacheco, D. Rodr´ıgues, Y. Y. Yang, A. N. Deshmukh, D. R. Mendes Jr., V. Morcelle, V. Scarduelli, and D. S. Monteiro, Elastic and inelastic scattering for the ^{11}B + ^{58}Ni system: Target and projectile reorientation effects, PHYSICAL REVIEW C 92, 054615 (2015).

[64] Gomes, P. R. S., Lubian, J., Canto, L. F., Otomar, D. R., Junior, D. M., de Faria, P. N., and Hussein, M. S. (2016). Reactions with weakly bound nuclei, at near barrier energies, and the breakup and transfer influences on the fusion and elastic scattering. *few-body Systems*, *57*(3), 165-176.

[65] Yang, Y. Y., Liu, X and Pang, D. Y. (2016). Distinction between elastic scattering of weakly bound proton-and neutron-rich nuclei: The case of ^{8}B and ^{11}Be. *Physical Review C*, *94*(3), 034614.

[66] Scarduelli, V., Crema, E., Guimarães, V., Abriola, D., Arazi, A., de Barbará, E., and Monteiro, D. S. (2017). Elastic and inelastic scattering for the ^{10}B + ^{58}Ni system at near-barrier energies. *Physical Review C*, *96*(5), 054610.

[67] Carlson, B. V., Frederico, T., and Hussein, M. S. (2017). Inclusive breakup of three-fragment weakly bound nuclei. *Physics Letters B*, *767*, 53-57.

[68] Pérez, R. N., and and Lei, J. (2019). Is the unusual near-threshold potential behavior in elastic scattering of weakly-bound nuclei a precision error?. *Physics Letters B*, *795*, 200-205.

[69] Fonseca, L. M., Linares, R., Zagatto, V. A. B., Cappuzzello, F., Carbone, D., Cavallaro, M., and Oliveira, J. R. B. (2019). Elastic and inelastic scattering of ^{16}O on ^{27}Al and ^{28}Si at 240 MeV. *Physical Review C*, *100*(1), 014604.

[70] Hassan, A. J., and Jassim, K. S. (2020). Effect of Surface Diffuseness Parameter on Quasi-elastic Scattering Calculations for ^{6}He+ ^{64}Zn, ^{7}Li+ ^{64}Zn and ^{8}Li+ ^{90}Zr Systems. *NeuroQuantology*, *18*(9), 40.

[71] Taylor, J. R. (1972). Scattering theory: the quantum theory on nonrelativistic collisions (John Wiley and Sons), INC. New York.

[72] Koelink, E. (2009). Scattering theory, M.Sc. Thesis, Radbound Universiteit Nijmegen.

[73] Paetz gen. Schieck, H., and Paetz gen. Schieck, H. (2014). Nuclear Astrophysics. *Nuclear Reactions: An Introduction*, 231-240.

[74] Popovicz Seidel, E., and Arretche, F. (2019). Zero range potential approximation in quantum scattering problems. *American Journal of Physics*, *87*(10), 796-801.

[75] Schröder, W. U., and Huizenga, J. R. (1984). Treatise on Heavy-Ion Science. *ed. DA Bromley*, *2*.

[76] Toke, J., and Schroder, W. U. (1992). Excitation energy division in dissipative heavy-ion collisions. *Annual Review of Nuclear and Particle Science*, *42*(1), 401-446.

[77] Krane, K. S., and Halliday, D. (1988). *Introductory nuclear physics* (Vol. 465). New York: Wiley.

[78] Reuss, P. (2008). Neutron physics.

[79] Leo, W. R. (1994). *Techniques for Nuclear and Particle Physics Experiments: A How-To Approach*. Springer Science and Business Media.

[80] Scherzinger, J. (2016). *Neutron Irradiation Techniques*. Lund University.

[81] NG Sjostrand. Reaktorfysik - forelasningar av professor N.G. Sjostrand, Chalmers University of Technology(1996).

[82] Weber, M. and Herlitzius, C. (2010). Gra. Lab. Exp., 52, 1.

[83] Paetz gen. Schieck, H., and Paetz gen. Schieck, H. (2014). Nuclear Astrophysics. *Nuclear Reactions: An Introduction*, 231-240.

[84] Lilley, J. S. (2001). Nuclear Physics: Principles and Applications. *Nuclear Physics: Principles and Applications*, 412.

[85] Satchler, G. R. (1990). *Introduction to nuclear reactions*. Macmillan International Higher Education.

[86] Joachain, C. J. (1975).Quantum Collision Theory (North-Holland Publishing Company).

[87] Wong, S. S. (2008). *Introductory nuclear physics*. John Wiley and Sons. D. J. Griffiths, Introduction to Quantum Mechanics (Pearson Eduction, Inc), (2005).

[88] Paar, H. (2010). *An introduction to advanced quantum physics*. John Wiley and Sons.

[89] Rodberg, L. S., Thaler, R. M., and Thaler, R. M. (1967). *Introduction to the quantum theory of scattering* (Vol. 26). Academic Press.

[90] M. Weber and C. Herlitzius, Gra. Lab. Exp., 52, 1 (2010).

[91] Schiff, L. I. (1949). *A Textbook of Quantum Mechanics*. McGraw-Hill Book Company.

[92] Ziock, K. (1969). *Basic quantum mechanics*. Wiley.

[93] Esposito, G., Marmo, G., Miele, G., and Sudarshan, G. (2015). *Advanced Concepts in Quantum Mechanics*. Cambridge University Press.

[94] Park, D. (1974). Introduction to the quantum theory.

[95] Arfken, G. (1985), Mathematical Methods for Physicsts (Academic Press, Inc.).

[96] Dasgupta, M., Hinde, D. J., Newton, J. O., and Hagino, K. (2004). The nuclear potential in heavy-ion fusion. *Progress of Theoretical Physics Supplement*, *154*, 209-216.

[97] Hagino, K., and Takigawa, N. (2012). Subbarrier fusion reactions and many-particle quantum tunneling. *Progress of theoretical physics*, *128*(6), 1061-1106.

[98] M. L. B. I. Ibrahim, PhD thesis, University of Malaya Kuala Lumpur, (2012).

[99] Fröbrich, P., and Lipperheide, R. (1996). *Theory of nuclear reactions* (Vol. 18). Courier Corporation.

[100] Merzbacher, E. Quantum mechanics (J. Wiley, 1970).

[101] Kamimura, M., Yahiro, M., Iseri, Y., Sakuragi, Y., Kameyama, H., and Kawai, M. (1986). Coupled-channels theory of breakup processes in nuclear reactions. *Prog. Theor. Phys. Suppl*, *89*(1).

[102] Austern, N., Iseri, Y., Kamimura, M., Kawai, M., Rawitscher, G., and Yahiro, M. (1987). Continuum-discretized coupled-channels calculations for three-body models of deuteron-nucleus reactions. *Physics Reports*, *154*(3), 125-204.

[103] Giles, M. (1988). *Non-reflecting boundary conditions for the Euler equations*. Computational Fluid Dynamics Laboratory, Department of Aeronautics and Astronautics, Massachusetts Institute of Technology.

[104] Balantekin, A. B., DeWeerd, A. J., and Kuyucak, S. (1996). Relations between fusion cross sections and average angular momenta. *Physical Review C*, *54*(4), 1853.

[105] Hagino, K., and Takigawa, N. (2012). Subbarrier fusion reactions and many-particle quantum tunneling. *Progress of theoretical physics*, *128*(6), 1061-1106.

[106] Bosch, H. S., and Hale, G. M. (1992). Improved formulas for fusion cross-sections and thermal reactivities. *Nuclear fusion*, *32*(4), 611.

[107] Timmers, H., Leigh, J. R., Dasgupta, M., Hinde, D. J., Lemmon, R. C., Mein, J. C., and Rowley, N. (1995). Probing fusion barrier distributions with quasi-elastic scattering. *Nuclear Physics A*, *584*(1), 190-204.

[108] Brink, D. M. (1985). Semi-classical methods for nucleus-nucleus scattering.

[109] Landowne, S., and Wolter, H. H. (1981). On sub-Coulomb heavy-ion scattering and the problem of nuclear absorption. *Nuclear Physics A*, *351*(1), 171-188.

[110] Brink, D. M., and Satchler, G. R. (1981). The role of the attractive nuclear potential in determining reaction cross sections. *Journal of Physics G: Nuclear Physics*, *7*(1), 43.

[111] Hagino, K., and Rowley, N. (2004). Large-angle scattering and quasielastic barrier distributions. *Physical Review C*, *69*(5), 054610.

[112] Rowley, N., Satchler, G. R., and Stelson, P. H. (1991). On the "distribution of barriers" interpretation of heavy-ion fusion. *Physics Letters B*, *254*(1-2), 25-29.

[113] Andres, M. V., Rowley, N., and Nagarajan, M. A. (1988). Effect of deformation on the elastic and quasielastic scattering of heavy ions near the Coulomb barrier. *Physics Letters B*, *202*(3), 292-295.

[114] Kruppa, A. T., Romain, P., Nagarajan, M. A., and Rowley, N. (1993). Effect of multiphonon coupling on heavy-ion fusion. *Nuclear Physics A*, *560*(3), 845-862.

[115] Timmers, H., Leigh, J. R., Dasgupta, M., Hinde, D. J., Lemmon, R. C., Mein, J. C., and Rowley, N. (1995). Probing fusion barrier distributions with quasi-elastic scattering. *Nuclear Physics A*, *584*(1), 190-204.

[116] Cochran, W. G. (1952). The $\chi 2$ test of goodness of fit. *The Annals of mathematical statistics*, 315-345.

[117] Mohr, P., de Faria, P. N., Lichtenthäler, R., Pires, K. C. C., Guimaraes, V., Lépine-Szily, A., and Morais, M. C. (2010). Comparison of ^{120}Sn (^{6}He, ^{6}He) ^{120}Sn and^{120}Sn (α, α) Sn 120 elastic scattering and signatures of the ^{6}He neutron halo in the optical potential. *Physical Review C*, *82*(4), 044606.

[118] Fernández-García, J. P., Zadro, M., Di Pietro, A., Figuera, P., Fisichella, M., Lattuada, M., and Torresi, D. (2015, March). Coupling to continuum effects in the $^{6,\ 7}$Li+ ^{64}Zn reactions at energies around the Coulomb barrier. In *Journal of Physics: Conference Series* (Vol. 590, No. 1, p. 012040). IOP Publishing.

[119] Lubian, J., Correa, T., Aguilera, E. F., Canto, L. F., Gomez-Camacho, A., Quiroz, E. M. and Gomes, P. R. S. (2009). Effects of breakup couplings on ^{8}B + ^{58}Ni elastic scattering. *Physical Review C*, *79*(6), 064605.

[120] P. R. S. Gomes, M. D. Rodriguez, C. V. Marti, I. Padron, L. C. Chamon, J. O. Fernandez Niello, O. A. Capurro, A. J. Pacheco, J. E. Testoni, A. Arazi, M. Ramirez, R. M. Anjos, J. Lubian, R. Viega, R. Liguori Neto, E. Crema, N. Added, C. Tenreiro, M. S. Hussein,(2005) Effect of the break-up on the fusion and elastic scattering of weakly bound projectiles on ^{64}Zn, Phys. Rev. C 71, 034608.

[121] Wang, N. and Scheid, W. (2008). Quasi-elastic scattering and fusion with a modified Woods-Saxon potential. *Physical Review C*, *78*(1), 014607.

[122] Kolata, J. J., Guimarães, V. and Aguilera, E. F. (2016). Elastic scattering, fusion, and breakup of light exotic nuclei. *The European Physical Journal A*, *52*(5), 1-38.

[123] Pesudo, V., Borge, M. J. G., Moro, A. M., Lay, J. A., Nácher, E., Gómez-Camacho, J. and Wang, Z. M. (2017). Scattering of the Halo Nucleus Be 11 on Au 197 at Energies around the Coulomb Barrier. *Physical review letters*, *118*(15), 152502.

الخلاصة

في هذه الرسالة، الحسابات للمقاطع العرضية بالاستطارة النووية الكلية المتضمنة (المرنة والغير مرنة) والتوزيع لحاجز كولوم اخذت للنوى الضعيفة الترابط لبعض الأنظمة المختارة هي:

$^{6}He + ^{120}Sn$, $^{6}Li + ^{64}Zn$, $^{7}Li + ^{64}Zn$, $^{8}B + ^{58}Ni$, $^{9}Be + ^{64}Zn$, $^{12}C + ^{208}Pb$, $^{6}He + ^{58}Ni$ and $^{11}Be + ^{197}Au$.

تم تحقيق التأثير لقنوات الاقتران مع قناة التفكك على الحسابات للنسبة بين المقاطع العرضية للاستطارة الكلية مع مقاطع استطارة رذرفورد σ_T/σ_R بالإضافة لتوزيع الحاجز D_{el} (MeV^{-1}).

تم وصف الجهد النووي البصري باستخدام جهد وود ساكسون Wood-Saxon (WS) الذي يحوي بارامترات الجزء (الحقيقي والخيالي) وهي العمق، نصف القطر ومعامل انتشار السطح النووي. اخذت بارامترات جهد النووي Wood-Saxon لجهد Akyüz-Winther بواسطة طريقة اقل المربعات للقيم العملية لمقاطع الاستطارة العرضية بواسطة برنامج فرعي كتب بلغة الفورتران90.

الكود المبرمج CC-SCT الذي يعتبر النسخة الاحدث لكود CC الذي برمج بلغة فورتران 90 . هذا البرنامج درس التهيجات الكولومية لتفاعلات الاستطارة في الميكانيك الكمي باستخدام طريقة القنوات المقترنة المتقطعة- المستمرة CDCC، لنظرية Alder and Winther.

حسابات النسبة بين المقاطع العرضية للاستطارة النووية الى مقاطع استطارة رذرفورد كدالة لمركز كتلة الزاوية θ_{cm} ومركز كتلة الطاقة E_{cm} بالإضافة الى حساب توزيع الاستطارة المرنة كدالة للطاقة D_{el} في حالات الاقتران وعدم الاقتران في توافق جيد مع القيم العملية المتوفرة يرجع لدور الاقتران مع قناة التفكك. القيم الافضل للبارا مترات نفذت من خلال التوافق الجيد بين الحسابات مع البيانات العملية.

جمهورية العراق

وزارة التعليم العالي والبحث العلمي

جامعة بابل

كلية التربية للعلوم الصرفة

قسم الفيزياء

تاثير أقتران القنوات في الاستطارة المرنه و غير المرنه للنوى ضعيفة الترابط لبعض الانظمة المختارة

رسالة مقدمة

الى مجلس كلية التربية للعلوم الصرفة في جامعة بابل

وهي جزء من متطلبات نيل درجة الماجستير

في التربية / الفيزياء

من قبل الطالبة

ايمان دعبول عبدالحمزه كاظم

بأشراف

أ.د. فؤاد عطيه مجيد **أ.د.فاطمه محمد حسين**

1443 هـ **2021 م**